Detection of race-specific resistance against *Puccinia coronata* f. sp. *avenae* in *Brachypodium* species

Vahid Omidvar, Sheshanka Dugyala, Feng Li, Susan Rottschaefer, Marisa E. Miller, Mick Ayliffe, Matthew J. Moscou, Shahryar F. Kianian, Melania Figueroa.

First, second, third, fourth, fifth, eighth and ninth authors: Plant Pathology, University of Minnesota, St. Paul, MN, USA; sixth author: CSIRO Agriculture and Food, ACT, Australia; seventh author: The Sainsbury Laboratory, Norwich Research Park, Norwich NR4 7UH, UK; eighth author: Cereal Disease Laboratory, United States Department of Agriculture-Agricultural Research Service, St. Paul, MN, USA; ninth author: Stakman-Borlaug Center for Sustainable Plant Health, University of Minnesota, St. Paul, MN, USA.

Correspondence: Melania Figueroa; email: figue031@umn.edu; Tel: +1 612 624 2291

Abstract

Oat crown rust caused by *Puccinia coronata* f. sp*. avenae* is the most destructive foliar disease of cultivated oat. Characterization of genetic factors controlling resistance responses to *Puccinia coronata* f. sp*. avenae* in non-host species could provide new resources for developing disease protection strategies in oat. We examined symptom development and fungal colonization levels of a collection of *Brachypodium distachyon* and *B. hybridum* accessions infected with three North American *P. coronata* f. sp*. avenae* isolates. Our results demonstrated that colonization phenotypes are dependent on both host and pathogen genotypes, indicating a role for race-specific responses in these interactions. These responses were independent of the accumulation of reactive oxygen species. Expression analysis of several defense-related genes suggested that salicylic acid and ethylene-mediated signaling, but not jasmonic acid are components of resistance reaction to *P. coronata* f. sp*. avenae*. Our findings provide the basis to conduct a genetic inheritance study to examine if effector-triggered immunity contributes to non-host resistance to *P. coronata* f. sp*. avenae* in *Brachypodium* species.

Keywords non-host, oat, crown rust, resistance, susceptibility, effector

Introduction

Oat crown rust caused by the obligate biotrophic rust fungus *Puccinia coronata* f. sp. *avenae* is the most widespread and damaging foliar disease of cultivated oat (*Avena sativa* L.) (Nazareno et al. 2017). Symptoms of crown rust infection manifest in the foliar tissue, causing a reduction in photosynthetic capacity and thus affecting grain size and quality (Holland and Munkvold 2001; Simons 1985). The most sustainable method to control this devastating disease is the use of genetic resistance (Carson 2011). Novel sources of genetic resistance may therefore translate into novel crop protection strategies.

In general, plant disease resistance to would-be pathogens can be conferred by either constitutive or induced barriers (Heath 2000; Nurnberger and Lipka 2005). Physical barriers, such as rigid cell walls and waxy cuticles as well as preformed antimicrobial compounds are some of the constitutive obstacles that explain why plants are immune to most microbes. Nevertheless, certain microbes have evolved strategies to overcome these barriers, and in such instances plant-microbe incompatibility is based upon pathogen recognition and the induction of plant defense responses (Heath 2000, Periyannan et al. 2017).

Inducible defense responses in plants are mediated by a tightly regulated two-tier immune recognition system that, depending on the physiological characteristics of the potential pathogen, may or may not be effective at preventing microbial colonization (Dodds and

74 Rathjen 2010). The first layer of microbial recognition is controlled by cell surface
75 associated receptors, named pattern recognition receptors (PRRs). PRRs recognize
76 conserved and essential microbial molecules known as pathogen-associated molecular
77 patterns (PAMPs) and/or plant derived damage-associated molecular patterns (DAMPs).
78 This recognition leads to the activation of a range of broad-spectrum basal defenses that
79 constitute PAMP-triggered immunity (PTI) (Zipfel 2008). PAMPs in pathogenic fungi like
80 the crown rust pathogen include chitin or xylanases, which are essential constituents of
81 the fungal cell wall. In contrast, DAMPs are not necessarily pathogen derived and include
82 plant cell wall fragments and plant peptides released during infection.
83
84 Adapted pathogens manipulate PTI signaling events and suppress basal defenses by
85 secreting a suite of effector proteins into plant cells, thereby enabling successful plant
86 colonization in some instances (Toruno et al. 2016). However, disease resistance against
87 adapted pathogens can still occur if the plant can recognize one or more of these secreted
88 effector molecules. Effector recognition generally occurs by plant intracellular nucleotide
89 binding leucine rich repeat (NB-LRR) receptors that each induce defense responses upon
90 recognition of a cognate pathogen effector, also known as an avirulence (Avr) protein.
91 This second layer of pathogen recognition, referred to as effector-triggered immunity
92 (ETI), frequently results in a localized hypersensitive cell death response at attempted
93 infection sites (HR) and is the underlying molecular basis of the gene-for-gene concept
94 (Dodds and Rathjen 2010; Ellis et al. 2014; Flor 1971). ETI is highly specific with
95 resistance only occurring if the adapted pathogen isolate expresses an effector that is
96 recognized by a corresponding NB-LRR in the infected plant.

The delivery of rust effector proteins into host plants is mediated by distinct fungal infection structures called haustoria (Catanzariti et al. 2006; Garnica et al. 2014; Panstruga and Dodds 2009). Only a small number of effectors have been characterized in rust fungi (Chen et al. 2017; Maia et al. 2017; Ravensdale et al. 2011; Salcedo et al. 2017), however, genome-wide effector mining suggests that rust pathogens may deploy hundreds of effector molecules via the haustorium during infection (Cantu et al. 2013; Duplessis et al. 2011; Hacquard et al. 2012; Nemri et al. 2014; Rutter et al. 2017). Oat crown rust populations are typified by a complex race-structure, which likely originates from variation in the array of effectors present in different pathogen genotypes (Carson 2011; Chong et al. 2000; Nazareno et al. 2017). For years, oat breeding programs have relied upon naturally occurring resistance in *Avena* spp., most likely mediated by *NB-LRR* genes, to protect against crown rust. However, the resistance of these oat varieties is often rapidly overcome by evolution of the crown rust pathogen to avoid host plant recognition. Achieving increased durability in oat crown rust resistance therefore requires new sources of genetic immunity to be identified and further advances made in our understanding of the molecular basis of rust recognition in host and non-host plant species.

Non-host plant species potentially offer an untapped resistance resource. Non-host resistance (NHR) is typically described in the context of a dichotomy that distinguishes it from host resistance. NHR is defined as genotype-independent and effective against all genetic variants of a non-adapted pathogen species, whereas host resistance is

120 genotype-dependent and effective only against a subset of genetic variants of an adapted
121 pathogen (Mysore and Ryu 2004). This paradigm has been gradually changing as
122 accumulating evidence suggests that signaling pathways and defense mechanisms
123 overlap in non-host and host resistance and that microbial adaptation to plant species
124 does not conform to a simple qualitative distinction (Bettgenhaeuser et al. 2014; Dawson
125 et al. 2015; Figueroa et al. 2015; Gill et al. 2015; Thordal-Christensen 2003). Instead,
126 disease phenotypes observed for different plant and pathogen interactions span a
127 continuous spectrum of outcomes ranging from immunity to susceptibility, with many
128 intermediate interactions, making the classification of non-host versus host systems
129 problematic (Bettgenhaeuser et al. 2014; Dawson et al. 2015). Regardless of the
130 terminology, identifying the molecular determinants of non-host or intermediate
131 resistance is of great interest as this type of resistance could be durable and broad-
132 spectrum and contribute significantly to crop improvement.
133
134 *Brachypodium distachyon,* a small grass closely related to cereals, is considered a non-
135 host to several rust fungi species related to *P. coronata* f. sp*. avenae*, such as *Puccinia*
136 *emaculata*, *Puccinia striiformis, Puccinia graminis* and *Puccinia triticina* (Ayliffe et al.
137 2013; Barbieri et al. 2011; Bettgenhaeuser et al. 2014; Bossolini et al. 2007; Dawson et
138 al. 2015; Figueroa et al. 2013, 2015; Gill et al. 2015). Variation in fungal colonization in
139 some of these interactions suggests that it may be possible to genetically dissect these
140 types of immune responses and harness them for engineering rust disease resistance
141 (Figueroa et al. 2015). In this study, we examined the interaction between *P. coronata* f.
142 sp*. avenae* and *B. distachyon*, as well as *Brachypodium hybridum*. *B. hybridum* is an

143 allotetraploid species originated from the hybridization of the diploid species *B. distachyon*
144 *and B. stacei* (Lopez-Alvarez et al. 2012).
145
146 Pathogen susceptibility in plants, particularly to rust fungi, is a process, which remains
147 poorly characterized. Our study shows that *P. coronata* f. sp. *avenae* can infect *B.*
148 *distachyon* and *B. hybridum* leaves and grow extensively, but cannot sporulate. These
149 findings open the possibility of investigating mechanisms that confer partial rust
150 susceptibility in *Brachypodium.* Gene expression analysis of an ortholog of the putative
151 rust susceptibility factor in wheat, which encodes a hexose transporter (Moore et al.
152 2015), suggested that sugar transport may also be important to sustain the growth of *P.*
153 *coronata* f. sp. *avenae* in *B. distachyon.* In addition to this, we found evidence for race-
154 specific resistance in both species supporting the model proposed by Schulze-Lefert and
155 Panstruga (2011), which postulates a role of ETI in NHR due to the phylogenetic
156 relatedness between the non-host and host species. These findings provide a framework
157 to conduct genetic inheritance studies to dissect recognition of *P. coronata* f. sp. *avenae*
158 by *B. distachyon* and *B. hybridum* and identify loci governing intermediate oat crown rust
159 susceptibility.
160
161 **Materials and Methods**
162
163 **Plant and fungal materials**
164
165 Twenty-two accessions of *B. distachyon* (ABR6, ABR7, Adi12, Adi13, Adi15, Bd1-1,

Bd18-1, Bd21, Bd21-3, Bd2-3, Bd29-1, Bd30-1, Bd3-1, BdTR10H, BdTR13K, Foz1, J6.2, Jer1, Koz5, Luc1, Mon3, and Tek4) and three accessions of *B. hybridum* (Bou1, Bel1, and Pob1) were used in this study. Seeds were obtained from the John Innes Centre (Dawson et al. 2015), Aberystwyth University (Mur et al. 2011), Joint Genome Institute and Montana State University (Vogel et al. 2009), Universidad Politécnica de Madrid (Dr. Elena Benavente) and USDA-ARS Plant Science Unit, St. Paul, MN, U.S.A (Garvin et al. 2008). All plants were increased by single seed descent prior to conducting this study. The cultivated oat (*Avena sativa*) variety Marvelous was used as a susceptible host to *P. coronata* f. sp*. avenae*. This study used three North American oat crown rust isolates, 12NC29 (race LBBB) and 12SD80 (race STTG) (Miller et al. 2018) collected in 2012, and a historic race 203 (race QBQT) known to be avirulent to the oat variety Victoria (Chang and Sadanaga 1964). Isolates were obtained from the rust collection available at the USDA-ARS Cereal Disease Laboratory, St. Paul, MN, U.S.A., and physiological race analysis was conducted following a standard nomenclature system using a set of oat differentials (Chong et al. 2000; Nazareno et al. 2017). Reported race assignment conveys consistent results from three independent experiments. Virulence phenotypes of *P. coronata* f. sp*. avenae* isolates on oat differentials with infection types of “0”, “0;”, “;”, “;C”, “1;”, “1”, “2”, “3”, “3+”, and “4” were converted to a 0-9 numeric scale, respectively for heat map generation.

Inoculation and pathogen assays

Brachypodium and oat seedlings were grown with 18/6 h light/dark, 24/18°C day/night

cycles and 50% humidity. Urediniospores were activated by heat shock treatment at 45ºC for 15 min to break cold induced dormancy and suspended in an oil carrier (Isopar M, ExxonMobil) for spray inoculation. Seedlings of *Brachypodium* accessions and oat were inoculated using 50 µL of each *P. coronata* f. sp*. avenae* inoculum (10 mg urediniospores/mL) at three-leaf and first-leaf stages, respectively. For mock inoculation, seedlings were sprayed with oil without urediniospores. Infected seedlings were placed in dew chambers in the dark for 12 h with intermittent misting for 2 min every 30 min. After 12 h, misting was stopped and seedlings were exposed to light for 2 h before they were placed back in growth chambers. Infected primary leaves of oat and secondary leaves of *Brachypodium* accessions were collected for analysis. Presence (+) or absence (-) of macroscopic symptoms, including chlorosis and/or necrosis as well as severity of the symptoms (shown as increments of +) were evaluated at 14 days post infection (dpi) in two independent experiments (biological replicates). Each biological replicate simultaneously tested all accessions, and five plants were examined per accession. Each plant was considered a technical replicate within one independent experiment. Digital images were captured using a stereomicroscope (Olympus model SZX16). To examine correlations between necrosis or chlorosis and estimates of fungal colonization (mean values), symptoms described as “-”, “+”, “++”, “+++” and “++++” were transformed to numerical values 0-4, respectively, to calculate a Spearman’s rank correlation coefficient.

Analysis of fungal colonization by microscopy

Both infected secondary *Brachypodium* leaves at 14 dpi and infected primary *A. sativa*

(variety Marvelous) leaves at 12 dpi were cut into 1 cm length sections and stained with wheat germ agglutinin Alexa Fluor® 488 conjugate (WGA-FITC; ThermoFisher Scientific) to visualize fungal colonies as previously described (Ayliffe et al. 2013; Dawson et al. 2015). Visualization of fungal intracellular growth was carried out using a fluorescence microscope (Leica model DMLB) under blue light with a 450-490 nM excitation filter. The percentage of leaf colonized (pCOL) by *P. coronata* f. sp. *avenae* was estimated according to the method of Dawson et al. (2015) with a modification to report 0, 0.5, 0.75, and 1 scores for disjointed fields of view with hyphal growth less than 15%, between 15-50%, 50-75%, and greater than 75%, respectively. Two independent experiments (biological replicates) were evaluated per *P. coronata* f. sp. *avenae* isolate (12SD80, 203, and 12NC29) and each biological replicate included three leaves. Each leaf was considered a technical replicate within one independent experiment. pCOL values from all three leaves were combined to obtain a mean and standard error of the mean. Fungal development was also examined in whole-mounted infected leaves of *B. distachyon* accessions ABR6 and Bd21 and oat at 1, 2, 3, and 6 dpi. The percentage of urediniospores that successfully germinated and formation of various infection structures, including appresorium (AP), substomatal vesicle (SV), haustorium-mother cell (HMC), and established colonies (EC), were recorded in WGA-FITC stained samples. Three independent experiments (biological replicates) were conducted and simultaneously evaluated infections with *P. coronata* f. sp. *avenae* isolates 12SD80, 203, and 12NC29. Each biological replicate recorded fungal development for 100 infection sites. Mean and standard error of the mean per infection structure category were calculated based on all three biological replicates.

Analysis of H_2O_2 accumulation

H_2O_2 accumulation was evaluated using 3,3′-diaminobenzidine (DAB) staining as described by Thordal-Christensen et al. (1997). Infected leaves were stained in 1 mg/mL DAB aqueous solution at pH 3.8 for 4 h in dark and destained in Farmer's fixative for 12 h. Three independent experiments (biological replicates) were conducted. Each biological replicate included one to two infected secondary leaves to record the number of urediniospores from a 100 sample within a 500 µm distance to a DAB staining site at 2, 4 and 6 dpi. The oat differential that contains the resistance gene *Pc91*, which confers resistance to rust isolates 12SD80 and 12NC29, was included as a positive experimental control for detection of H_2O_2. Three negative controls were used including an oat differential that contains the resistance gene *Pc14* which is not effective against 12SD80 and 12NC29, oat variety Marvelous infected with 12SD80 and 12NC29 and mock inoculated Marvelous. Samples were examined using an upright light microscope (Nikon Eclipse 90i). Mean and standard error of the mean of the number of urediniospores associated with H_2O_2 accumulation were calculated based on all three biological replicates. Digital micrographs were captured with a Nikon D2-Fi2 color camera using bright field and objective lens 4x and 10x. Multiple images were acquired in X, Y and Z planes using Z-series process using the Nikon Elements software. Z-stacking images were treated with an extended depth of focus (EDF) function to focus all the planes.

qPCR quantification of fungal DNA

Genomic DNA was extracted from infected and mock-treated secondary leaves of *B. distachyon* accessions ABR6 and Bd21 at 3, 7, and 12 dpi using DNeasy Plant Mini Kit (Qiagen). The relative abundance of fungal DNA was measured using the Femto™ Fungal DNA Quantification Kit (Zymo Research) based on quantification of ITS regions using ITS-specific primers and fungal DNA Standards provided by the manufacturer. PCR was conducted using a CFX96 Real-Time system (Bio-Rad) and thermal cycles were set for initial denaturation at 95°C for 10 min, 45 cycles of 95°C for 30 s, 50°C for 30 s, 60°C for 60 s, followed by a final extension cycle at 72°C for 7 min. The *Brachypodium GAPDH* gene was also quantified in the same DNA samples using gene-specific primers (Hong et al. 2008). Fungal DNA level was normalized relative to the plant *GAPDH* value in each sample. Four independent experiments (biological replicates) were analyzed per time point per isolate, with two technical replicates within each biological replicate. Mean and standard error of the mean per condition (fungal isolate x *Brachypodium* accession x time point) were calculated based on data from all four experiments. Correlation between accumulation of fungal DNA, combined for all isolates at each time point (3, 7, and 12 dpi) and estimates of fungal colonization, combined for all isolates at 14 dpi was determined using a Pearson's correlation coefficient test.

RNA extraction and RT-qPCR analysis

Total RNA was extracted from infected and mock-treated secondary leaves of *B. distachyon* accessions ABR6 and Bd21 at 12, 24, 48, and 72 hpi using the RNeasy Plant Mini Kit (Qiagen). For RT-qPCR, cDNA was synthesized using the PrimeScript First

Strand cDNA Synthesis Kit (Takara) and amplification was performed using the SensiFAST SYBR Lo-ROX Kit (Bioline). Sequences of gene-specific primers, reported by Gill et al. (2015) and Mandadi and Scholthof (2012) and those used in our study are listed in Supplementary Table 1. The *GAPDH*, *Ubi4* and *Ubi18* genes were examined as potential reference genes (Hong et al. 2008). Expression levels were normalized using the plant *GAPDH* gene after comparing PCR efficiencies and variation of quantification cycle (Cq) values for all three genes across time points in mock or pathogen-inoculated *Brachypodium* accessions (ABR6 and Bd21). PCR thermal cycles were set for initial denaturation at 95°C for 2 min, 40 cycles of 95°C for 5 s, followed by annealing/extension at 60°C for 20 s in a CFX96 Real-Time PCR system (Bio-Rad). Data was collected from three independent experiments (biological replicates) and each biological replicate included two technical replicates. Differential expression (DE) values were calculated as normalized fold changes of the expression using the ΔΔCT method (Livak and Schmittgen 2001), and DE value ≥ 2 was considered as a significant change in gene expression.

Results

Variation in resistance response of *Brachypodium* accessions to *P. coronata* f. sp. *avenae* infection

To examine the ability of *P. coronata* f. sp. *avenae* to infect non-host species *B. distachyon* and *B. hybridum* we evaluated the disease responses of 25 different *Brachypodium* accessions to three North American *P. coronata* f. sp. *avenae* isolates,

12SD80, 203, and 12NC29. First we characterized the virulence phenotypes of these isolates using a set of oat differentials (Fig. 1A). All three isolates are fully virulent on the susceptible oat variety Marvelous with obvious sporulation occurring at 14 dpi (Fig 1B, C). In contrast, no pustules were observed on any *Brachypodium* accession 30 days post-infection, which suggests that the asexual phase of the *P. coronata* f. sp. *avenae* life cycle cannot be completed on either *B. distachyon* or *B. hybridum.* However, macroscopic symptoms were observed on *Brachypodium* accessions in response to challenge with these rust isolates (Fig. 1D, E, Table 1) with some accessions developing chlorosis and/or necrosis of varying severity (Fig. 1F, Table 1). These symptoms were dependent upon both the accession genotype and rust genotype. For example, the necrosis severity of accession Bd1-1 was high in response to isolate 12SD80 but low upon infection with isolates 203 and 12NC29, whereas chlorosis severity in accession Adi13 was higher when challenged with isolates 12SD80 and 12NC29 but lower in response to isolate 203. Some *Brachypodium* accessions, such as Bd2-3, Bd3-1 and Tek4, reacted differently to all three rust isolates with different necrosis and chlorosis severities observed in each interaction. ABR6 consistently showed minimal symptom development, whereas accessions such as Bd21, Bd21-3 and Koz5 displayed more extreme necrosis and chlorosis responses to all three isolates.

In parallel, all accessions were analyzed microscopically to determine the extent of *P. coronata* f. sp. *avenae* infection for each isolate. For all three isolates, urediniospores germinated to produce appressoria and penetrated the plant indicating that *Brachypodium* accessions are recognized as a potential host by *P. coronata* f. sp. *avenae*

(Supplementary Fig. 1). A large variation in rust growth was observed amongst these *Brachypodium* accessions (Fig. 2A) although growth was always less than that observed on the oat host. Microscopically no *P. coronata* f. sp. *avenae* isolate showed initiation of uredinia on any *Brachypodium* accession confirming the non-host status of *B. distachyon* and *B. hybridum* to this phytopathogen.

In general, *P. coronata* f. sp. *avenae* isolates 12SD80 and 203, which are more broadly virulent on the oat differentials (27 and 12, respectively) than isolate 12NC29 (5), showed more extensive growth on all tested *Brachypodium* accessions (Fig. 2A). Maximum colonization was greatest for isolate 12SD80, which colonized ~79% of the leaf area of accession Bd21-3, while isolate 203 colonized ~64% of the leaf area of accession Adi15. In contrast, the maximum colonization for isolate 12NC29 was ~41% of the leaf area of accession Koz5. For all three isolates, Koz5 and Bd21-3 were amongst those *B. distachyon* accessions with the greatest fungal growth, whereas *B. distachyon* accessions ABR6 and Foz1, as well as *B. hybridum* accession Pob1, had the least fungal growth.

The fungal growth of each isolate and accession combination was scored relative to the most fungal growth observed for each isolate (Supplementary Fig. 2). Interestingly, some accessions (i.e., Bd30-1, Bd3-1, BdTR10H) were substantially infected by isolates 12SD80 and 203 while growth of 12NC29 was more restricted. In contrast, accession Tek4 was similarly infected by isolates 12SD80 and 12NC29, but had greater growth of 203, while isolate 12SD80 grew more prolifically on accession Mon3 than did either

isolates 203 and 12NC29. Remarkably, we did not observe a correlation between the degree of necrosis and fungal colonization levels for each isolate (rho= 0.39-0.44, *p*=0.03-0.05, Spearman's test). Weak correlations were found between chlorosis and colonization levels of 12SD80 (rho= 0.62, *p*=1.37e-06) and 203 (rho= 0.53, *p*=0.0064), in contrast to 12NC29 (rho= 0.30, *p*=0.15). For example, Bd29-1 showed extensive necrosis and chlorosis when inoculated with isolate 12SD80 in contrast to 203, but had high levels of colonization by both isolates. Accession Bd18-1 developed the highest necrosis and chlorosis in response to 12NC29 but supported the lowest growth of this isolate. In contrast, the most obvious symptoms on Jer1 correlated with the greatest fungal growth, in this case by isolate 12SD80.

The variation in fungal growth occurring on different *Brachypodium* accessions suggests that it may be possible to dissect the genetic architecture controlling this NHR against *P. coronata* f. sp. *avenae*. Given the availability of an ABR6 x Bd21 $F_{4:5}$ *B. distachyon* family (Bettgenhaeuser et al. 2017) and the differences observed in *P. coronata* f. sp. *avenae* infection patterns (Fig. 2A), these two parental accessions were further analyzed. To further confirm the colonization values estimated for ABR6 and Bd21, fungal DNA accumulation was quantified by qPCR for each rust isolate over a time course experiment of 3, 7 and 12 dpi (Fig. 2B). Fungal DNA levels of each isolate increased in both accessions; however, statistical significant differences in the accumulation of DNA were observed between accessions at 7 and 12 dpi. Fungal DNA abundance was higher in accession Bd21 for all three isolates compared with ABR6, while isolate 12NC29 had the least growth on both accessions. A strong correlation was observed between levels of

373 fungal colonization of all three isolates in ABR6 and Bd21 and their fungal DNA
374 abundance at 7 dpi (r=0.93, *p*=0.0056, Pearson's test) and 12 dpi (r=0.91, *p*=0.0098),
375 while the correlation was not significant at 3 dpi (r=0.76, *p*=0.07). These results validate
376 fungal colonization estimates shown in Fig. 2A.
377
378 **Development of infection structures of *P. coronata* f. sp. *avenae* isolates on *B.**
379 ***distachyon* ABR6 and Bd21**
380
381 The development of infection structures (Fig. 3A) of isolates 12SD80, 203, and 12NC29
382 in a time course experiment (1, 2, 3, and 6 dpi) was compared between ABR6 and Bd21,
383 with the susceptible oat variety Marvelous included as a positive control. Spore
384 germination rates (GS) and appressorium development (AP) of all three rust isolates were
385 similar on ABR6, Bd21 and oat (Fig. 3B). However, fungal growth on both *Brachypodium*
386 accessions was significantly slower than on susceptible oat, with fewer substomatal
387 vesicles (SV), haustorium-mother cells (HMC) and established colonies (EC) produced
388 at 1, 2 and 3 dpi. The infection progression was generally slower on accession ABR6 than
389 Bd21, while isolate 12SD80 grew at a faster rate on *B. distachyon* compared with the
390 other two isolates, as demonstrated by the increased percentage of infection sites that
391 formed SV in both accessions at 1 dpi. The most noticeable differences in the parental
392 accessions ABR6 and Bd21 were related to the development of SV at 2 dpi with isolate
393 12SD80 and HMC at 3 dpi for isolates 12SD80 and 203.
394
395 **Histological analysis of reactive oxygen species in *B. distachyon* ABR6 and Bd21**

The accumulation of H_2O_2 in mesophyll cells was examined by DAB staining in accessions ABR6 and Bd21 upon infection with isolates 12SD80, 203, and 12NC29 at 2, 4, and 6 dpi (Table 2, Supplementary Fig. 3). We conducted three independent experiments examining in each case 100 urediniospores from all three rust isolates. For isolate 12SD80 we found only a small number of urediniospores within 500 µm distance to DAB sites in ABR6 and Bd21, with slightly higher numbers of DAB sites in ABR6 than in Bd21 at 2 dpi and 4 dpi (Table 2). In contrast, DAB accumulation was rare in response to isolates 203 and 12NC29. We used an oat line carrying the *Pc91* gene, which confers resistance against 12SD80 and 12NC29 isolates (Fig. 1A), as a positive experimental control. In this case we observed a significantly greater proportion of urediniospores (~50-60%) from 12SD80 and 12NC29 in association with H_2O_2 accumulation sites. The staining intensity and size of the H_2O_2 accumulation sites were also greater in the positive control samples than those in ABR6 and Bd21 (Supplementary Fig. 3). The resistance gene *Pc14*, which is not effective against 12SD80 and 12NC29 isolates, susceptible oat Marvelous infected with 12SD80 and 12NC29 (Fig. 1A) and mock inoculated Marvelous were used as negative controls and did not result in accumulation of H_2O_2 (Table 2, Supplementary Fig. 3). These data suggest that H_2O_2 accumulation is not a common feature of *B. distachyon* NHR to *P. coronata* f. sp. *avenae.*

Transcript profiling of defense-related genes in *B. distachyon* ABR6 and Bd21

To investigate the role of phytohormone-dependent defense responses in *Brachypodium*

upon *P. coronata* f. sp. *avenae* infection, the temporal expression profile of several defense-related genes involved in SA, ET, and JA signaling pathways, as well as genes involved in callose synthesis and the phenylpropanoid pathway, were examined. This analysis was undertaken for ABR6 and Bd21 during the early stages of infection (up to 3 dpi), when there were not significant differences in fungal growth among isolates in both accessions (Fig. 2B). Three possible references genes were evaluated for data normalization, *GAPDH, Ubi4* and *Ubi18* (Hong et al. 2008). qRT-PCR primers for the *GAPDH* gene showed the highest amplification efficiency (98.4%) when compared to primers for *Ubi4* (96%) and *Ubi18* (97.1%) (Supplementary Fig. 4A). The *GAPDH* gene was selected for data normalization as it displayed the least variation in expression (Cq values) when compared to *Ubi4* and *Ubi18* in mock and fungal infected tissues in both *B. distachyon* accessions and all time points together (Supplementary Fig. 4B). *GAPDH* displayed steady expression in mock and infected tissues across time points in each accession (Supplementary Fig. 4C) which further supported the suitability of this gene for data normalization. In general, expression of genes involved in the SA and ET signaling pathways were induced in ABR6 and Bd21 during the first 48 h post-infection; however, expression of JA biosynthesis genes was not altered (Fig. 4, Supplementary Fig. 5). Changes in gene expression were greater in ABR6 than Bd21 upon infection with isolates 12SD80 and 203, but the inverse was observed for isolate 12NC29. These findings suggest differences between ABR6 and Bd21 in the early signaling responses to *P. coronata* f. sp. *avenae* infection.

Among the SA signaling pathway genes, expression of *Aberrant Growth Defects 2*

(*AGD2*) peaked at 24 to 48 hpi with isolates 12SD80, 203 and 12NC29. The highest upregulation of *AGD2* was observed in the interaction of 12SD80 and ABR6. Expression of *Alternative Oxidase* (*AOX1A*) was induced in ABR6 as early as 12 hpi with isolates 12SD80 and 203, but it was not affected in response to isolate 12NC29. In contrast, *AOX1A* was upregulated in Bd21 only at 48 hpi in response to isolates 12SD80 and 12NC29. The *Pathogenesis-related* (*PR*) genes *PR1* and *PR5* showed the greatest induction amongst all genes tested in response to all three crown rust isolates. The expression of both genes peaked at 48 hpi except for *PR5* expression after inoculation with 12NC29 which peaked at 24 hpi. Overall, induction of these SA-responsive genes occurred in all interactions, but were remarkably stronger in ABR6 when inoculated with 12SD80 and 203, while Bd21 showed similar responses to all three isolates.

Expression of *Ethylene Response Factor 1* (*ERF1*) was maximal at 24 hpi with all three isolates and, as observed for SA-responsive genes, expression of *ERF1* was particularly high in ABR6 in response to isolates 12SD80 and 203. However, expression of an ET biosynthesis gene, *Aminocyclopropane-1-carboxylic Acid Oxidase* (*ACO1*), two JA biosynthesis genes, *Lipoxygenase 2* (*LOX2*), and *12-oxophytodienoate Reductase 3* (*OPR3*), *WRKY18* transcription factor, and *callose synthase* did not change in either of the accessions in response to challenge with any of the three isolates (Supplementary Fig. 5). Expression of *Phenylalanine Ammonia-Lyase* (*PAL*) was only slightly induced in ABR6 at 12 hpi with isolate 12SD80. *Cinnamyl Alcohol Dehydrogenase* (*CAD*) reached maximum induction in both accessions at 24 to 48 hpi with isolates 12SD80 and 203. In response to infection with isolate 12NC29, this gene was only upregulated in Bd21

between 24 to 48 hpi.

Transcript profiling of *BdSTP13* in *B. distachyon* ABR6 and Bd21

The expression of the *Brachypodium* ortholog of *Lr67 (STP13)* (Bradi1g69710) (Moore et al. 2015) was examined in accessions ABR6 and Bd21 upon infection with all three rust isolates, as it acts as a putative hexose transporter. *BdSTP13* was induced in both accessions in response to the tested rust isolates (Fig. 5). Gene induction peaked at 24 to 48 hpi, except in the interaction between ABR6 and12NC29, which showed low *BdSTP13* transcript accumulation.

Discussion

The lack of effective *P. coronata* f. sp. *avenae* resistance in oat coupled with rapid evolution of pathogen virulence necessitates a search for new sources of resistance to control oat crown rust disease. To explore the potential of using *Brachypodium* species as a germplasm resource for disease resistance against *P. coronata* f. sp. *avenae*, we have characterized the interaction between three *P. coronata* f. sp. *avenae* isolates and a panel of *Brachypodium* accessions, including *B. distachyo*n and *B. hybridum*. At the macroscopic level, variation in resistance phenotypes was observed, which has been previously reported for other rust interactions with *B. distachyon.* In these studies, *P. striiformis*, *P. graminis*, and *P. triticina* infection phenotypes varied from immunity to a range of symptoms that included pustule formation and sporulation (Ayliffe et al. 2013;

Figueroa et al. 2013; Garvin 2011). However, similar to *Brachypodium-P. emaculata* (switchgrass rust) interactions (Gill et al. 2015), we did not observe *P. coronata* f. sp. *avenae* sporulation on any *Brachypodium* accession, which supports the status of *B. distachyon* and *B. hybridum* as non-hosts for this pathogen. Macroscopic infection symptoms were often associated with chlorosis and/or necrosis; however, it was visually difficult to confirm if these symptoms were a consequence of *P. coronata* f. sp. *avenae* infection. Microscopic analysis showed that *P. coronata* f. sp. *avenae* isolates 12SD80, 203, and 12NC29 overcame pre-haustorial resistance defenses and were able to colonize leaves of all *Brachypodium* accessions tested. These results are similar to the interactions observed between *P. graminis* f. sp. *tritici* and *B. distachyon* (Ayliffe et al. 2013). In light of these observations, we would like to emphasize that our definition of *B. distachyon* and *B. hybridum* as non-hosts is based on previous established terminology, which uses absence of sporulation as indicator of resistance. However, given that both species tolerate growth of *P. coronata* f. sp. *avenae*, both *B. distachyon* and *B. hybridum* could be considered as non-native hosts, and previous observations reflect also variations in susceptibility. Furthermore, changes in growth conditions may favor sporulation of *P. coronata* f. sp. *avenae* in both *B. distachyon* and *B. hybridum.*

To better understand the phenotypic variation existing between *P. coronata* f. sp. *avenae and Brachypodium* interactions, we compared the extent of fungal growth on a range of accessions. The rust isolates included in this study represent three distinct physiological races (genotypes). A wide range of pathogen growth was observed on different *Brachypodium* accessions and was dependent on both plant and fungal genotypes. Some

511 *Brachypodium* accessions tolerated more fungal growth when infected with isolates
512 12SD80 and 203 versus 12NC29 (i.e., Bd30-1, Bd3-1, BdTR10H) (Fig. 2, Supplementary
513 Fig. 2). Interestingly, we also identified accessions (i.e., Tek4) that tolerated more growth
514 of isolates 12SD80 and 12NC29 than 203. These findings could be explained either by
515 the lack of a plant target for pathogen effectors to promote infection effectively or the
516 presence of race-specific components to resistance. The latter scenario implies that
517 resistance is likely governed by variation in effector repertoires of the rust isolates and *R*
518 genes present in the *Brachypodium* accessions. Given the close evolutionary relationship
519 between oat and *Brachypodium* spp., it is possible that the accessions included in our
520 study carry *R* genes that can detect effectors of *P. coronata* f. sp. *avenae.* Isolates
521 12SD80 and 12NC29 display different virulence profiles on the oat differential set and the
522 recent sequencing of these isolates provides evidence of extensive differences in effector
523 gene complements of 12SD80 and 12NC29 (Miller et al. 2018). Future studies identifying
524 and comparing the effector repertoires of rust species, including those in our study and
525 others that infect *Brachypodium* (i.e., *Puccinia brachypodii*) may help to explain our
526 findings.
527
528 The precise contribution of ETI to non-host rust resistance in *Brachypodium* remains
529 elusive. Future efforts to dissect the genetic factors controlling resistance to *P. coronata*
530 f. sp. *avenae* in *B. distachyon* will help to evaluate the model proposed by Schulze-Lefert
531 and Panstruga (2011), in which ETI is the major contributor to NHR in plant species that
532 are closely related to the natural host. Heterologous expression of fungal and bacterial
533 effectors in several non-host pathosystems supports that effector recognition by

534 immunoreceptors contributes to resistance (Adlung et al. 2016; Giesbers et al. 2017; Lee
535 et al. 2014; Stassen et al. 2013; Sumit et al. 2012), although in some cases effector
536 recognition can occur in the absence of resistance (Giesbers et al. 2017; Goritschnig et
537 al. 2012). Close examination of *Brachypodium* interactions with *P. graminis* ff. spp. *tritici*,
538 *avena* and *phalaridis*, *P. triticina*, and *P. striiformis* suggests that HR-induced cell death
539 is rare (Ayliffe et al. 2013). However, the lack of HR in these interactions does not
540 necessarily undermine the contribution of ETI to non-host resistance, as there are
541 instances when *R* gene-mediated ETI (e.g., wheat stem rust resistance gene, *Sr33*) can
542 result in resistance without cell death (Periyannan et al. 2013). Further studies are needed
543 to better understand the extent of ETI and HR contributions in NHR given that molecular
544 and genetic factors in these interactions could be pathosystem-specific.
545
546 To investigate the role of ROS in *B. distachyon* response to *P. coronata* f. sp. *avenae,* we
547 examined accumulation of ROS in accessions ABR6 and Bd21, which display contrasting
548 infection phenotypes. We found a small number of urediniospores from 12SD80
549 associated with ROS accumulation, while detection of ROS was rare for other two
550 isolates. However in these cases the accumulation of ROS in ABR6 and Bd21 was
551 substantially less than that detected in a resistant oat line carrying the resistance gene
552 *Pc91* (Table 2). These findings make the involvement of this ROS unlikely in the
553 resistance of *Brachypodium* to *P. coronata* f. sp. *avenae.* In contrast to H_2O_2,
554 phytohormones may play a thus far undefined role in modulating NHR in *Brachypodium*
555 to rust pathogens.
556

Plant responses to pathogens are partly regulated through a complex interplay between salicylic acid (SA), ethylene (ET) and jasmonic acid (JA) signaling pathways (Denancé et al. 2013). Gill et al. (2015) found that several defense-related genes involved in SA, ET, and JA signaling pathways were induced in *Brachypodium* accessions infected with *P. emaculata*. In our study, upregulation of several SA-responsive genes and the key ethylene response regulator *ERF1* was detected, suggesting that SA and ET-signaling pathways may positively regulate NHR against *P. coronata* f. sp. *avenae*. The *Pathogenesis-related* (*PR*) genes *PR1* and *PR5* were upregulated in response to all rust isolates and given that *PR1* is a key marker gene of SA signaling (Kouzai et al. 2016; Sels et al. 2008), this further supports that the activation of SA-dependent defense responses may contribute to the phenotypes observed in *B. distachyon* and *B. hybridum* during *P. coronata* f. sp. *avenae* infection. JA biosynthesis genes were not induced, making this hormone unlikely to play an active role in this NHR response. In contrast, *ERF1*, which acts as a key regulatory element in the ET/JA-dependent defense responses, was upregulated suggesting that ET-responsive genes may enhance NHR (Berrocal-Lobo et al. 2002; Lorenzo et al. 2003; Müller and Munné-Bosch 2015). *Phenylalanine Ammonia-Lyase* (*PAL*) is a key enzyme in biosynthesis of polyphenolic compounds and lignin precursors and is often associated with host resistance responses against pathogens (Kalisz et al. 2015). Lignin deposition in response to pathogen attack is usually correlated with reinforcement of the cell wall and enhanced resistance (Miedes et al. 2014). Upregulation of *PAL* does not appear to play a significant role in the responses of *B. distachyon* to *P. coronata* f. sp. *avenae;* however, induction of *CAD* may point to cell wall alterations in response to isolates 12SD80 and 203. A genome-wide

580 transcriptional analysis of the interaction of *P. coronata* f. sp. *avenae* with ABR6 and Bd21
581 will help to elucidate the involvement of some of these specific processes in NHR,
582 including phytohormone regulation.
583
584 Extensive *P. coronata* f. sp. *avenae* growth in some *Brachypodium* accessions implies
585 that the pathogen is capable of nutrient accession for a period of time and possibly able
586 to target susceptibility factors conserved between *Brachypodium* and oat. Little is known
587 about the mechanisms underlying rust susceptibility. Pathogens can alter sugar
588 partitioning in the host to accommodate their growth (Lapin and Van den Ackerveken
589 2013), and thus sugar transporter proteins (STPs) may be targeted by rust fungi to
590 increase nutrient availability (Dodds and Lagudah 2016). The wheat *STP13* hexose
591 transporter is implicated in supporting rust pathogens as mutations in this gene leads to
592 broad-spectrum resistance (Moore et al. 2015). We examined the expression of the
593 ortholog of wheat *STP13* in *Brachypodium* during infection by *P. coronata* f. sp. *avenae*.
594 Interestingly, the highest levels of *BdSTP13* expression were obtained in accession Bd21,
595 which is subjected to more rust growth than ABR6, suggesting that the gene may indeed
596 serve as a susceptibility factor. Our results are consistent with previous findings that show
597 that expression of *Lr67,* and its homoeologs in wheat peaks at 24 hpi upon infection with
598 the leaf rust fungus, *Puccinia triticina*. Gene expression analysis of *Lr67* as well as other
599 *STP13* genes in *Arabidopsis* and grapevine, indicates that the gene is also induced in
600 response to pathogens (Hayes et al. 2010; Lemonnier et al. 2014; Moore et al. 2015).
601 These observations provide a basis to study the contribution of sugar transport to rust
602 susceptibility in an experimental system that is not as complex as in hexaploid oat and

603 wheat.

604

605 Several studies have demonstrated the value of mining wild relatives of crop species to
606 introduce disease resistance. Effective race-specific rust resistance has been
607 introgressed into wheat (*Triticum aestivum*) from related species, such as the *Sr50* gene
608 from rye (*Secale cereale*), which confers resistance to wheat stem rust by recognition of
609 the corresponding AvrSr50 effector of *P. graminis* f. sp. *tritici* (Chen et al. 2017; Mago et
610 al. 2015). Similarly, functional transfer of the pigeonpea (*Cajanus cajan*) *CcRpp1*
611 resistance gene into soybean confers resistance against soybean rust (*Phakopsora*
612 *pachyrhizi*), which demonstrates how heterologous resistance transgenes can be used
613 for crop improvement (Kawashima et al. 2016). This interspecies transfer of disease
614 resistance highlights the possibility that *Brachypodium* genes that confer NHR to *P.*
615 *coronata* f. sp. *avenae* could potentially be transferred to oat and provide disease
616 resistance. As a next step, we are utilizing an ABR6 x Bd21 mapping population to identify
617 resistance loci that could be tested in *A. sativa*. Both accumulation of fungal DNA and
618 analysis of development of fungal infection structures (i.e., SV or HCM) can be used to
619 phenotype the ABR6 x Bd21 mapping population. In summary, our findings indicate that
620 *Brachypodium* is a suitable species for evaluating NHR to *P. coronata* f. sp. *avenae* and
621 is a potential source of novel disease resistance for oat. The rapid expansion of genomic
622 resources, including fully sequenced genomes and assessment of genetic diversity
623 among *Brachypodium* genotypes (International *Brachypodium* Initiative 2010; Gordon et
624 al. 2014, 2017) enables this species to be exploited for engineering disease resistance in
625 closely related crop species.

Acknowledgements

We acknowledge support by the University of Minnesota Experimental Station USDA-NIFA Hatch/Figueroa project MIN-22-058, as well as the USDA-ARS-The University of Minnesota Standard Cooperative Agreement (3002-11031-00053115) between S.F.K and M.F. M.J.M. is supported by the Gatsby Foundation and Biotechnology and Biological Sciences Research Council (BB/P012574/1). We thank P.N. Dodds and E. Henningsen for discussions and comments during manuscript preparation, as well as Roger Caspers and Lief van Lierop for technical support. We would like to acknowledge the University Imaging Centers (UIC) (http://uic.umn.edu) and staff support at the University of Minnesota for using microscopy equipment.

638 **Literature cited**

639

640 Adlung, N., Prochaska, H., Thieme, S., Banik, A., Blüher, D., John, P., et al. 2016. Non-
641 host resistance induced by the Xanthomonas effector XopQ is widespread within the
642 genus Nicotiana and functionally depends on EDS1. Front. Plant Sci. 7.

643

644 Ayliffe, M., Singh, D., Park, R., Moscou, M.J., and Pryor, T. 2013. The infection of
645 *Brachypodium distachyon* with selected grass rust pathogens. Mol. Plant Microbe
646 Interact. 26:946-957.

647

648 Barbieri, M., Marcel, T.C., and Niks, R.E. 2011. Host status of false brome grass to the
649 leaf rust fungus *Puccinia brachypodii* and the stripe rust fungus *P. striiformis.* Plant Dis.
650 95:1339-1345.

651

652 Berrocal-Lobo, M., Molina, A., and Solano, R. 2002. Constitutive expression of
653 ETHYLENE-RESPONSE-FACTOR1 in *Arabidopsis* confers resistance to several
654 necrotrophic fungi. Plant J. 29:23-32.

655

656 Bettgenhaeuser, J., Gilbert, B., Ayliffe, M., and Moscou, M. J. 2014. Nonhost resistance
657 to rust pathogens–a continuation of continua. Front. Plant Sci. 5:664.

658

659 Bettgenhaeuser J, Corke, F.M.K., Opanowicz, M., Green, P., Hernández-Pinzón, I.,
660 Doonan, J.H., et al. 2017. Natural variation in *Brachypodium* links vernalization and

661 flowering time loci as major flowering determinants. Plant Physiol. 173:256-268.

662

663 Bossolini, E., Wicker, T., Knobel, P. A., and Keller, B. 2007. Comparison of orthologous
664 loci from small grass genomes *Brachypodium* and rice: implications for wheat genomics
665 and grass genome annotation. Plant J. 49:704-717.

666

667 Cantu, D., Segovia, V., MacLean, D., Bayles, R., Chen, X., Kamoun, S., et al. 2013.
668 Genome analyses of the wheat yellow (stripe) rust pathogen *Puccinia striiformis* f. sp.
669 *tritici* reveal polymorphic and haustorial expressed secreted proteins as candidate
670 effectors. BMC Genomics 14:270.

671

672 Carson, M.L. 2011. Virulence in oat crown rust (*Puccinia coronata* F. sp. *avenae*) in the
673 United States from 2006 through 2009. Plant Dis. 95:1528-1534.

674

675 Catanzariti, A.M., Dodds, P.N., Lawrence, G.J., Ayliffe, M.A., and Ellis, J.G. 2006.
676 Haustorially expressed secreted proteins from flax rust are highly enriched for avirulence
677 elicitors. Plant Cell 18:243-256.

678

679 Chang, T.D., and Sadmaga, K. 1964. Crosses of six rnonosomics in *Avena sativa* L. with
680 varieties, species and chlorophyll mutants. Crop Sci. 4: 589-593.

681

682 Chen, J., Upadhyaya, N.M., Ortiz, D., Sperschneider, J., Li, F., Bouton, C., et al. 2017.
683 Loss of *AvrSr50* by somatic exchange in stem rust leads to virulence for *Sr50* resistance

in wheat. Science 358:1607-1610.

Chong, J., Leonard, K.J., and Salmeron, J.J. 2000. A North American system of nomenclature for *Pucinia coronata* f.sp. *avenae*. Plant Dis. 84:580-585.

Dawson, A.M., Bettgenhaeuser, J., Gardiner, M., Green, P., Hernández-Pinzón, I., Hubbard, A., et al. 2015. The development of quick, robust, quantitative phenotypic assays for describing the host-nonhost landscape to stripe rust. Front. Plant Sci. 6:876.

Denancé, N., Sánchez-Vallet, A., Goffner, D., and Molina, A. 2013. Disease resistance or growth: the role of plant hormones in balancing immune responses and fitness costs. Front. Plant Sci. 4:155.

Dodds, P.N., and Rathjen, J.P. 2010. Plant immunity: towards an integrated view of plant-pathogen interactions. Nat. Rev. Genet. 11:539-548.

Dodds, P.N., and Lagudah, E.S. 2016. Starving the enemy. Science. 354:1377-1379.

Duplessis, S., Cuomob, C.A., Linc, Y.C., Aertsd, A., Tisseranta, E., Veneault-Fourreya, C., et al. 2011. Obligate biotrophy features unraveled by the genomic analysis of rust fungi. Proc. Natl. Acad. Sci. U.S.A. 108:9166-9171.

Ellis, J.G., Lagudah, E.S., Spielmeyer, W., and Dodds, P.N. 2014. The past, present and

707 future of breeding rust resistant wheat. Front. Plant Sci. 5:641.

708

709 Figueroa, M., Alderman, S., Garvin, D.F., and Pfender, W.F. 2013. Infection of
710 *Brachypodium distachyon* by formae speciales of *Puccinia graminis:* Early infection
711 events and host-pathogen incompatibility. PLoS One 8:e56857.

712

713 Figueroa, M., Castell-Miller, C.V., Li, F., Hulbert, S.H., and Bradeen, J.M. 2015. Pushing
714 the boundaries of resistance: insights from *Brachypodium*-rust interactions. Front. Plant
715 Sci. doi.org/10.3389/fpls.2015.00558.

716

717 Flor, H. 1971. Current status of the gene-for-gene concept. Annu. Rev. Phytopathol.
718 9:275-296.

719

720 Garnica, D.P., Nemri, A., Upadhyaya, N.M., Rathjen, J.P., and Dodds, P.N. 2014. The ins
721 and outs of rust haustoria. PLoS Pathog. 10:e1004329.

722

723 Garvin, D.F., Gu, Y.Q., Hasterok, R., Hazen, S.P., Jenkins, G., Mockler, T.C., et al.
724 2008. Development of genetic and genomic research resources for *Brachypodium*
725 *distachyon*, a new model system for grass crop research. Crop Sci. 48:S69-S84.

726

727 Garvin, D.F. 2011. Investigating rust resistance with the model grass *Brachypodium*, in
728 *Proceedings of the 2011 Borlaug Global Rust Initiative Technical Workshop,* June 13–19,
729 ed. R. McIntosh (St. Paul, MN), 89-91.

Giesbers, A.K.J., Pelgrom, A.J.E., Visser, R.G.F., Niks, R.E., Van den Ackerveken, G., and Jeuken, M.J.W. 2017. Effector-mediated discovery of a novel resistance gene against *Bremia lactucae* in a nonhost lettuce species. New Phytol. 216:915–926

Gill, U.S., Uppalapati, S.R., Nakashima, J., and Mysore, K.S. 2015. Characterization of *Brachypodium distachyon* as a nonhost model against switchgrass rust pathogen *Puccinia emaculata*. BMC Plant Biol. 15:113.

Gordon, S.P., Priest, H., Des Marais, D.L., Schackwitz, W., Figueroa, M., Martin, J., et al. 2014. Genome diversity in *Brachypodium distachyon*: Deep sequencing of highly diverse inbred lines. Plant J. 79:361-374.

Gordon, S.P., Contreras-Moreira, B., Woods, D.P., Des Marais, D.L., Burgess, D., Shu, S., et al. 2017. Extensive gene content variation in the *Brachypodium distachyon* pan-genome correlates with population structure. Nat. Commun. 8:2184.

Goritschnig, S., Krasileva, K.V., Dahlbeck, D., and Staskawicz, B.J. 2012. Computational prediction and molecular characterization of an oomycete effector and the cognate *Arabidopsis* resistance gene. PLoS Genet 8: e1002502.

Hacquard, S., Joly, D.L., Lin, Y.C., Tisserant, E., Feau, N., Delaruelle C., et al. 2012. A comprehensive analysis of genes encoding small secreted proteins identifies candidate

753 effectors in *Melampsora larici-populina* (Poplar Leaf Rust). Mol. Plant Microbe Interact.
754 25:279-293.
755
756 Hayes, M.A., Feechan, A., and Dry, I.B. 2010. Involvement of abscisic acid in the
757 coordinated regulation of a stress-inducible hexose transporter (VvHT5) and a cell wall
758 invertase in grapevine in response to biotrophic fungal infection. Plant Physiol. 153:211-
759 221.
760
761 Heath, M.C. 2000. Nonhost resistance and nonspecific plant defenses. Curr. Opin. Plant
762 Biol. 3:315-319.
763
764 Holland, J.B., and Munkvold, G.P. 2001. Genetic relationships of crown rust resistance,
765 grain yield, test weight, and seed weight in oat. Crop Sci. 41:1041-1050.
766
767 Hong, S.Y., Seo, P.J., Yang, M.S., Xiang, F., and Park, C.M. 2008. Exploring valid
768 reference genes for gene expression studies in *Brachypodium distachyon* by real-time
769 PCR. BMC plant biol. 8:112.
770
771
772 Kalisz, S., Oszmiański, J., and Wojdylo, A., 2015. Increased content of phenolic
773 compounds in pear leaves after infection by the pear rust pathogen. Physiol. Mol. Plant
774 Pathol. 91:113-119.
775

776 Kawashima, C.G., Guimaraes, G.A., Nogueira, S.R., MacLean, D., Cook, D.R.,
777 Steuernagel, B., et al. 2016. A pigeonpea gene confers resistance to Asian soybean rust
778 in soybean. Nat. Biotechnol. 34:661-665.
779
780 Kouzai, Y., Kimura, M., Yamanaka, Y., Watanabe, M., Matsui, H., and Yamamoto, M.
781 2016. Expression profiling of marker genes responsive to the defense-associated
782 phytohormones salicylic acid, jasmonic acid and ethylene in *Brachypodium distachyon*.
783 BMC Plant Biol. 16:59.
784
785 Lapin, D., and Van den Ackerveken, G. 2013. Susceptibility to plant disease: More than
786 a failure of host immunity. Trends Plant Sci. 18:546-554.
787
788 Lee, H. A., Kim, S. Y., Oh, S. K., Yeom, S. I., Kim, S. B., Kim, M. S., et al. 2014. Multiple
789 recognition of RXLR effectors is associated with nonhost resistance of pepper against
790 *Phytophthora infestans*. New Phytol. 203:926-938.
791
792 Lemonnier, P., Gaillard, C., Veillet, F., Verbeke, J., Lemoine, R., Coutos-Thévenot, P.,
793 et al. 2014. Expression of Arabidopsis sugar transport protein STP13 differentially affects
794 glucose transport activity and basal resistance to *Botrytis cinerea*. Plant Mol. Biol. 85:473-
795 484.
796
797 Livak, K.J., and Schmittgen, T.D. 2001. Analysis of relative gene expression data using
798 real-time quantitative PCR and the 2(-Delta Delta C(T)). Methods. 25:402-408.

Lopez-Alvarez, D., Lopez-Herranz, M.L., Betekhtin, A., and Catalan, P. 2012. A DNA barcoding method to discriminate between the model plant *Brachypodium distachyon* and its close relatives *B. stacei* and *B. hybridum* (Poaceae). PLoS One 7:e51058.

Lorenzo, O., Piqueras, R., Sánchez-Serrano, J.J., and Solano, R. 2003. ETHYLENE RESPONSE FACTOR1 Integrates Signals from Ethylene and Jasmonate Pathways in Plant Defense. Plant Cell. 15:165-178.

Mago, R., Zhang, P., Vautrin, S., Šimková, H., Bansal, U., Luo, M. C., et al. 2015. The wheat Sr50 gene reveals rich diversity at a cereal disease resistance locus. Nat. Plants. 1:15186.

Maia, T., Badel, J.L., Marin-Ramirez, G., Rocha, C.M., Fernandes, M.B., da Silva, J.C.F., et al. 2017. The *Hemileia vastatrix* effector HvEC-016 suppresses bacterial blight symptoms in coffee genotypes with the SH1 rust resistance gene. New Phytol. 213:1315-1329.

Mandadi, K.K. and Scholthof, K.B.G. 2012. Characterization of a viral synergism in the monocot *Brachypodium distachyon* reveals distinctly altered host molecular processes associated with disease. Plant Physiol. 160:1432-1452.

Miedes, E., Vanholme, R., Boerjan, W., and Molina, A. 2014. The role of the secondary

822 cell wall in plant resistance to pathogens. Front. Plant Sci. 5:358.

823

824 Miller, M. E., Zhang, Y., Omidvar, V., Sperschneider, J., Schwessinger, B., Raley, C., et
825 al. 2018. *De novo* assembly and phasing of dikaryotic genomes from two isolates of
826 *Puccinia coronata* f. sp. *avenae*, the causal agent of oat crown rust. mBio 9:e01650-17.

827

828 Moore, J.W., Herrera-Foessel, S., Lan, C., Schnippenkoetter, W., Ayliffe, M., Huerta-
829 Espino, J., et al. 2015. A recently evolved hexose transporter variant confers resistance
830 to multiple pathogens in wheat. Nat. Genet. 47:1494-1498.

831

832 Müller, M., and Munné-Bosch, S. 2015. Ethylene response factors: A key regulatory hub
833 in hormone and stress signaling. Plant Physiol. 169:32-41.

834

835 Mur, L.A., Allainguillaume, J., Catalan, P., Hasterok, R., Jenkins, G., Lesniewska, K.,
836 Thomas, L., and Vogel, J. 2011. Exploiting the *Brachypodium* tool box in cereal and grass
837 research. New Phytol. 191:334–347.

838

839 Mysore, K.S., and Ryu, C.M. 2004. Nonhost resistance: How much do we know? Trends
840 Plant Sci. 9:97-104.

841

842 Nazareno, E.S., Li, F., Smith, M., Park, R.F., Kianian, S.F., and Figueroa, M. 2017.
843 *Puccinia coronata* f. sp. *avenae*: a threat to global oat production. Mol. Plant Pathol. DOI:
844 10.1111/mpp.12608.

Nemri, A., Saunders, D.G.O., Anderson, C., Upadhyaya, N.M., Win, J., Lawrence, G.J., et al. 2014. The genome sequence and effector complement of the flax rust pathogen *Melampsora lini*. Front. Plant Sci. 5:98.

Nurnberger, T., and Lipka, V. 2005. Non-host resistance in plants: new insights into an old phenomenon. Mol. Plant Pathol. 6:335-345.

Panstruga, R., and Dodds, P.N. 2009. Terrific protein traffic: the mystery of effector protein delivery by filamentous plant pathogens. Science. 324:748-750.

Periyannan, S., Moore, J., Ayliffe, M., Bansal, U., Wang, X., Huang, L., et al. 2013. The gene *Sr33*, an ortholog of barley *Mla* genes, encodes resistance to wheat stem rust race Ug99. Science. 341:786-788.

Periyannan, S., Milne, R.J., Figueroa, M., Lagudah, E.S. and Dodds, P.N. 2017. An overview of genetic rust resistance: from broad to specific mechanisms. PLoS Pathog. 13: e1006380.

Ravensdale, M., Nemri, A., Thrall, P.H., Ellis J.G., and Dodds, P.N. 2011. Co-evolutionary interactions between host resistance and pathogen effector genes in flax rust disease. Mol. Plant Pathol. 12:93-102.

868 Rutter, W.B., Salcedo, A., Akhunova, A., He, F., Wang, S., Liang, H., et al. 2017.
869 Divergent and convergent modes of interaction between wheat and *Puccinia graminis* f.
870 sp. *tritici* isolates revealed by the comparative gene co-expression network and genome
871 analyses. BMC Genomics. 18:291.
872
873 Salcedo, A., Rutter, W., Wang, S., Akhunova, A., Bolus, S., Chao, S., et al. 2017.
874 Variation in the *AvrSr35* gene determines *Sr35* resistance against wheat stem rust race
875 Ug99. Science. 358:1604-1606.
876
877 Schulze-Lefert, P., and Panstruga, R. 2011. A molecular evolutionary concept connecting
878 nonhost resistance, pathogen host range, and pathogen speciation. Trends Plant Sci. 16:
879 117-125.
880
881 Sels, J., Mathys, J., De Coninck, B.M.A., Cammue, B.P.A., and De Bolle, M.F.C. 2008.
882 Plant pathogenesis-related (PR) proteins: A focus on PR peptides. Plant Physiol. Bioch.
883 46:941-950.
884
885 Simons, M.D. 1985. Crown rust. In: Roelfs AP, Bushnell WR (eds) The cereal rusts, vol.
886 II, disease, distribution, epidemiology and control. Academic, New York, USA, pp 131-
887 172.
888
889 Stassen, J. H. M., den Boer, E., Vergeer, P. W. J., Andel, A., Ellendorff, U., Pelgrom, K.,
890 et al. 2013. Specific in planta recognition of two GKLR proteins of the downy mildew

Bremia lactucae revealed in a large effector screen in lettuce. Mol. Plant. Microbe. Interact. 26:1259-70.

Sumit, R., Sahu, B. B., Xu, M., Sandhu, D., and Bhattacharyya, M. K. 2012. Arabidopsis nonhost resistance gene PSS1 confers immunity against an oomycete and a fungal pathogen but not a bacterial pathogen that cause diseases in soybean. BMC Plant Biol. 12:1.

The International *Brachypodium* Initiative. 2010. Genome sequencing and analysis of the model grass *Brachypodium distachyon*. Nature. 463:763-768.

Thordal-Christensen, H., Zhang, Z., Wei, Y., and Collinge, D.B. 1997. Subcellular localization of H_2O_2 in plants. H_2O_2 accumulation in papillae and hypersensitive response during the barley-powdery mildew interaction. Plant J. 11:1187-1194.

Thordal-Christensen, H. 2003. Fresh insights into processes of nonhost resistance. Curr. Opin. Plant Biol. 6:351-357.

Toruno, T.Y., Stergiopoulos, I., and Coaker, G. 2016. Plant-pathogen effectors: Cellular probes interfering with plant defenses in spatial and temporal manners. Annu. Rev. Phytopathol. 54:419-441.

914 Vogel, J.P., Tuna, M., Budak, H., Huo, N., Gu, Y.Q., and Steinwand, M.A. 2009.
915 Development of SSR markers and analysis of diversity in Turkish populations of
916 *Brachypodium distachyon*. BMC Plant Biol. 9:88.

917

918 Zipfel, C. 2008. Pattern-recognition receptors in plant innate immunity. Curr. Opin.
919 Immunol. 20:10-16.

920

Table 1. Variation of symptoms in *Brachypodium* accessions infected with *P. coronata* f. sp. *avenae* isolates.

	12SD80		203		12NC29	
Accessions	**Chlorosis**	**Necrosis**	**Chlorosis**	**Necrosis**	**Chlorosis**	**Necrosis**
ABR6	-	+	-	-	-	+
ABR7	+	+	+	+	+	+
Adi12	+++	+	++	+	+	+
Adi13	+++	++	+	+++	++++	++
Adi15	++	++	+++	+	+++	++
Bd1-1	+++	++++	+++	+	+	++
Bd18-1	-	+	+	+	+++	++
Bd21	++	+++	+++	+++	++	++
Bd21-3	++	+++	+++	++	++++	+++
Bd2-3	+++	+++	+	++	+	+
Bd29-1	++	++++	+	+	+	+++
Bd30-1	+	++	+	+	+	+++
Bd3-1	++	++++	+	+++	+++	++
BdTR10H	++	++	+	+	++	++
BdTR13K	+	++	+	++	+	++
Foz1	+	+	+++	++++	+	-
J6.2	+	+	+	+	+	+
Jer1	+	+++	-	+	+	++
Koz5	++	++	+++	++	+++	++
Luc1	+	+	+	-	++	+
Mon3	++	++++	+	+	+++	+
Tek4	-	+++	+	-	+	+
***Bel1**	+	++	+	+	+	++++
***Bou1**	+	+	+	++	-	+++
***Pob1**	-	+++	+	+	+	+

Accessions with asterisks correspond to *B. hybridum* and those without asterisk are *B. distachyon* accessions. Symbols “+” and “-” show presence or absence of macroscopic symptoms, respectively, and number of “+” indicates symptom severity with ++++ as maximum level.

Table 2. Histological analysis of H_2O_2 accumulation in *B. distachyon* accessions ABR6 and Bd21 and oat lines that contain the *Pc91* and Pc*14* genes in response to *P. coronata* f. sp. *avenae* infection.

Isolates	Plants	2 dpi	4 dpi	6 dpi
12SD80	ABR6	10.7 ± 1.8	8.7 ± 2	4.3 ± 1.2
	Bd21	4 ± 1.5	3.3 ± 0.9	3.7 ± 1.5
	* Susceptible oat (Marvelous)	0	0	0
203	ABR6	0	0.3 ± 0.3	1.7 ± 0.3
	Bd21	0	0	2 ± 0.6
	* Susceptible oat (Marvelous)	0	0	0
12NC29	ABR6	0	0.7 ± 0.3	1 ± 0.6
	Bd21	0.3 ± 0.3	0	1 ± 0.6
	* Susceptible oat (Marvelous)	0	0	0
12SD80	** Oat (*Pc91*)	61.3 ± 7.5	65 ± 4.9	47.7 ± 4.1
	* Oat (*Pc14*)	1 ± 0.6	0.3 ± 0.3	0.7 ± 0.7
12NC29	** Oat (*Pc91*)	56 ± 9.5	54 ± 6.4	49 ± 5.9
	* Oat (*Pc14*)	0	0.7 ± 0.3	0.7 ± 0.3

Values are calculated as means of three independent experiments, ± indicates standard error of the mean. Asterisks *, ** indicate negative and positive experimental controls, respectively.

Figure legends

Fig. 1. Infection of oat and *Brachypodium* accessions with *P. coronata* f. sp*. avenae.* **A**. Heat map of virulence phenotypes of *P. coronata* f. sp*. avenae* isolates on oat differentials. **B, C**. Formation of pustules and sporulation on infected susceptible oat leaves (Marvelous), respectively. **D, E**. Variation of infection symptoms and fungal colonization, respectively, on four *Brachypodium* accessions. **F**. Absence (-) or presence (+) of chlorosis and/or necrosis in *Brachypodium* accessions inoculated with *P. coronata* f. sp*. avenae* at 14 dpi. Level of symptom severity is indicated by the number of "+" characters. Symptoms correspond to the representative isolate 12SD80, except for the absence of necrosis which corresponds to isolate 203. Scale bars indicate 2 mm (B, D, F), 0.5 mm (C, top), 0.25 mm (C, bottom) and 0.5 mm (E)

Fig. 2. Colonization of *Brachypodium* accessions by *P. coronata* f. sp*. avenae*. **A**. Fungal growth estimates in foliar tissue for isolates 12SD80, 203, and 12NC29 depicted by the percentage of colonized area at 14 dpi. Crown rust susceptible oat (*A. sativa*) variety Marvelous serves as positive experimental control. Results from two independent experiments for each isolate are shown with distinct color intensities and each bar represents a mean value in one independent experiment (biological replicate). Error bars represent standard error of mean of three leaves (technical replicates) within one

974 independent experiment. **B**. Quantification of fungal DNA for each rust isolate in *B.*
975 *distachyon* accessions ABR6 (blue line) and Bd21 (orange line). Error bars represent
976 standard error of mean of four independent experiments (biological replicates).
977
978 **Fig. 3.** Fungal development of *P. coronata* f. sp*. avenae* in *Brachypodium* accessions. **A.**
979 Illustration of *P. coronata* f. sp*. avenae* development in the plant. Germinated
980 urediniospores (GS) form a penetration structure appressorium (AP) over a stoma. The
981 fungus enters the mesophyll cavity and differentiates a substomatal vesicle (SV) and
982 infection hypha. The establishment of a rust colony (EC) begins with the formation of a
983 feeding structure (haustorium) which requires differentiation of a haustorial mother cell
984 (HMC) near the hyphal tip. To undergo HMC formation, the rust fungus must come in
985 contact with a mesophyll cell. **B.** Bars show the percentage of interaction sites with
986 germinated urediniospores (GS, light blue), formation of appressorium (AP, orange),
987 substomatal vesicle (SV, gray), haustorium-mother cell (HMC, yellow), established colony
988 (EC, dark blue), and EC with sporulation (SP, green) in a sample of 100 infection sites
989 per independent experiment (biological replicate). Error bars represent standard error of
990 mean of three independent biological replicates.
991
992 **Fig. 4.** Expression profiling of various defense-related genes in *Brachypodium* accessions
993 in response to *P. coronata* f. sp*. avenae*. Gene expression (fold-change) relative to mock
994 inoculations in rust infected ABR6 (blue) and Bd21 (orange) plants of *Aberrant Growth*
995 *Defects* 2 (*AGD2*), *Alternative Oxidase* (*AOX1A*), *Pathogenesis-related* (*PR*) *genes,*
996 *Ethylene Response Factor* 1 (*ERF1*), *Phenylalanine Ammonia-Lyase* (*PAL*), and

997 *Cinnamyl Alcohol Dehydrogenase* (*CAD*). Barplots represent mean values of fold change
998 per time point. Solid colored bars indicate a fold change value of ≥ 2 whereas hatched
999 bars indicate values below this threshold. Error bars represent standard error of mean of
1000 of three independent experiments (biological replicates). Asterisks indicate statistically
1001 significant differences ($p \leq 0.05$) between ABR6 and Bd21 accessions as determined by
1002 a *t*-test.
1003
1004 **Fig. 5.** Expression profiling of *BdSTP13* in *Brachypodium* accessions in response to *P.*
1005 *coronata* f. sp*. avenae*. Gene expression (fold-change) relative to mock inoculations in
1006 rust infected ABR6 (blue) and Bd21 (orange) plants of the putative hexose transporter
1007 *BdSTP13.* Solid colored bars indicate a fold change value of ≥ 2 whereas hatched bars
1008 indicate values below this threshold. Error bars represent standard error of mean of three
1009 independent experiments (biological replicates) Asterisks indicate statistical significant
1010 differences ($p \leq 0.05$) between ABR6 and Bd21 accessions as determined by a *t*-test.
1011
1012 **Supplementary files**
1013
1014 **Supplementary Fig. 1** shows development of *P. coronata* f. sp*. avenae* in all
1015 *Brachypodium* accessions and susceptible oat Marvelous as quantified by percentage of
1016 germination, formation of appressorium and occurrence of plant penetration. Error bars
1017 represent standard error of mean of two independent experiments (biological replicates).
1018 Data was collected for 50 infection sites per independent biological replicate.
1019

Supplementary Fig. 2 shows colonization of *Brachypodium* accessions by *P. coronata* f. sp*. avenae*. Fungal growth estimate per isolate, with individual isolates 12SD80, 203 and 12NC29 shown as a percentage value relative to the accession displaying the highest level of colonization for each isolate.

Supplementary Fig. 3 shows examples of H_2O_2 detection at 2 dpi using DAB staining. Images depict urediniospores and presence of H_2O_2 is shown by a white arrow. **A, B, C.** *B. distachyon* accession ABR6 inoculated with rust isolates 12SD80, 203, and 12NC29, respectively. **D, E.** Oat differential line that contains the resistance gene *Pc91* inoculated with isolates 12SD80 and 12NC29, respectively. The gene *Pc91* is effective against both isolates and therefore serves as positive experimental control. **F, G.** Oat differential line that contains the resistance gene *Pc14* inoculated with isolates 12SD80 and 12NC29, respectively. The gene *Pc14* is not effective against any of the isolate and therefore serves as negative experimental control. **H, I.** Susceptible oat variety Marvelous inoculated with isolates 12SD80 and 12NC29, respectively. **J.** Lack of H_2O_2 in mock inoculated oat Marvelous (negative control). Scale bars indicate 100 µm.

Supplementary Fig. 4 shows evaluation of *GAPDH*, *Ubi4* and *Ubi18* as potential reference genes for data normalization in targeted gene expression analyses via qRT-PCR. **A.** Amplification efficiency of primers for *GAPDH*, *Ubi4* and *Ubi18* genes. **B**. Comparison of expression levels of *GAPDH*, *Ubi4*, and *Ubi18* genes between mock and pathogen-infected tissues after combining Cq values from both *B. distachyon* accessions (ABR6 and Bd21) and all time points (12, 24, 48, and 72 hpi). Boxplots show variation

between mean Cq values and whiskers on boxplots show variability outside the upper and lower quartiles. Data was collected from three independent experiments each including three technical replications. **C**. Comparison of expression levels of *GAPDH* in ABR6 and Bd21 in both mock and infected samples across time points. Graph shows mean values and error bars on dotplots represent standard error of mean of three independent experiments (biological replicates).

Supplementary Fig. 5 shows expression profiling of various defense-related genes in *B. distachyon* accessions in response to *P. coronata* f. sp*. avenae*. Gene expression (fold-change) relative to mock inoculations in rust infected ABR6 (blue) and Bd21 (orange) plants of *Aminocyclopropane-1-carboxylic Acid Oxidase* (*ACO1*), *Lipoxygenase 2* (*LOX2*), *12-oxophytodienoate Reductase 3* (*OPR3*), *WRKY18* transcription factor, and *callose synthase*. Barplots represent mean values of fold change per time point. Solid colored bars indicate a fold change value of ≥ 2 whereas hatched bars indicate values below this threshold. Error bars represent standard error of mean of three independent experiments (biological replicates). Asterisks indicate statistical significant differences ($p \leq 0.05$) between ABR6 and Bd21 accessions as determined by a *t*-test.

Supplementary Table 1. List of gene-specific primers used for RT-qPCR analysis.

Gene	Gene ID	Function	Primer (5´- 3´)
***AGD2**	Bradi3g49447	SA signaling	Forward: GTACCCAGAAGCGAAGGTCATC
			Reverse: TAGCCTTGGTAGCCTTCAGGAG
****AOX1A**	Bradi5g20547	SA signaling	Forward: ACTACGCCTCGGACATCCATTAC
			Reverse: AGGCATCGACCGTCCATTTGAG
****PR1**	Bradi1g57580	SA signaling	Forward: AGCTCTGGCATCATCAGCATCC
			Reverse: CGTTGTGTGGGTCCAGGAAATC
****PR5**	Bradi1g13060	SA signaling	Forward: CCGACCGATTACTCCAGGTTCTTC
			Reverse: TAATTAGCTCGCTCGCTCGCTTG
****ERF1**	Bradi3g50490	ET signaling	Forward: TGGTGCCGTGTGAAATTTGTCG
			Reverse: CAGATTTCGCTGCACCACTTGC
***ACO1**	Bradi1g75960	ET signaling	Forward: CATATTCCATCAGGGGAGAAGC
			Reverse: CTTCCACTGCCATACTCAGCAC
****LOX2**	Bradi3g07010	JA signaling	Forward: GCGGCGTTCGAGAAGTTCAATG
			Reverse: GTCCTGGTTATTGTTTCGCTCGTC
****OPR3**	Bradi1g05870	JA signaling	Forward: ACCCATTTCTTCTCGAATGATCCC
			Reverse: ACACGTGCAAGTACGGAAAGAAAG
***PAL**	Bradi3g49260	JA signaling	Forward: ATTCAGGCTATCCTTGCTGAGG
			Reverse: AGGAGCTTCCTTCCAAGATGTG
***WRKY18**	Bradi4g30360	Transcription factor	Forward: GCTTAGAGACGACGGCACTTAC
			Reverse: TTGATACCCATCCTTCACAACG
***CAD**	Bradi3g22980	Lignin biosynthesis	Forward: GGTACTGTCACCAAGGGAGG
			Reverse: GTGACCCAATCCCCCAAGTC
***CS**	Bradi2g46250	Callose biosynthesis	Forward: GGGAGCTTGCTACAATGGGT
			Reverse: TCACCACCACTTGTGTGCTT
***BdSTP13**	Bradi1g69710	Putative sugar transport	Forward: ATCTTCAATGGCGCTGCAC
			Reverse: GAAGAGGATGCCGATGGTGA
***GAPDH**	Bradi3g14120	Reference gene	Forward: TTGCTCTCCAGAGCGATGAC
			Reverse: CTCCACGACATAATCGGCAC

*,** Primer sequences were reported by Gill et al. (2015) and Mandadi and Scholthof (2012), respectively. Those that are not marked with asterisks were designed in our study.

Callose synthase is abbreviated as *CS.*

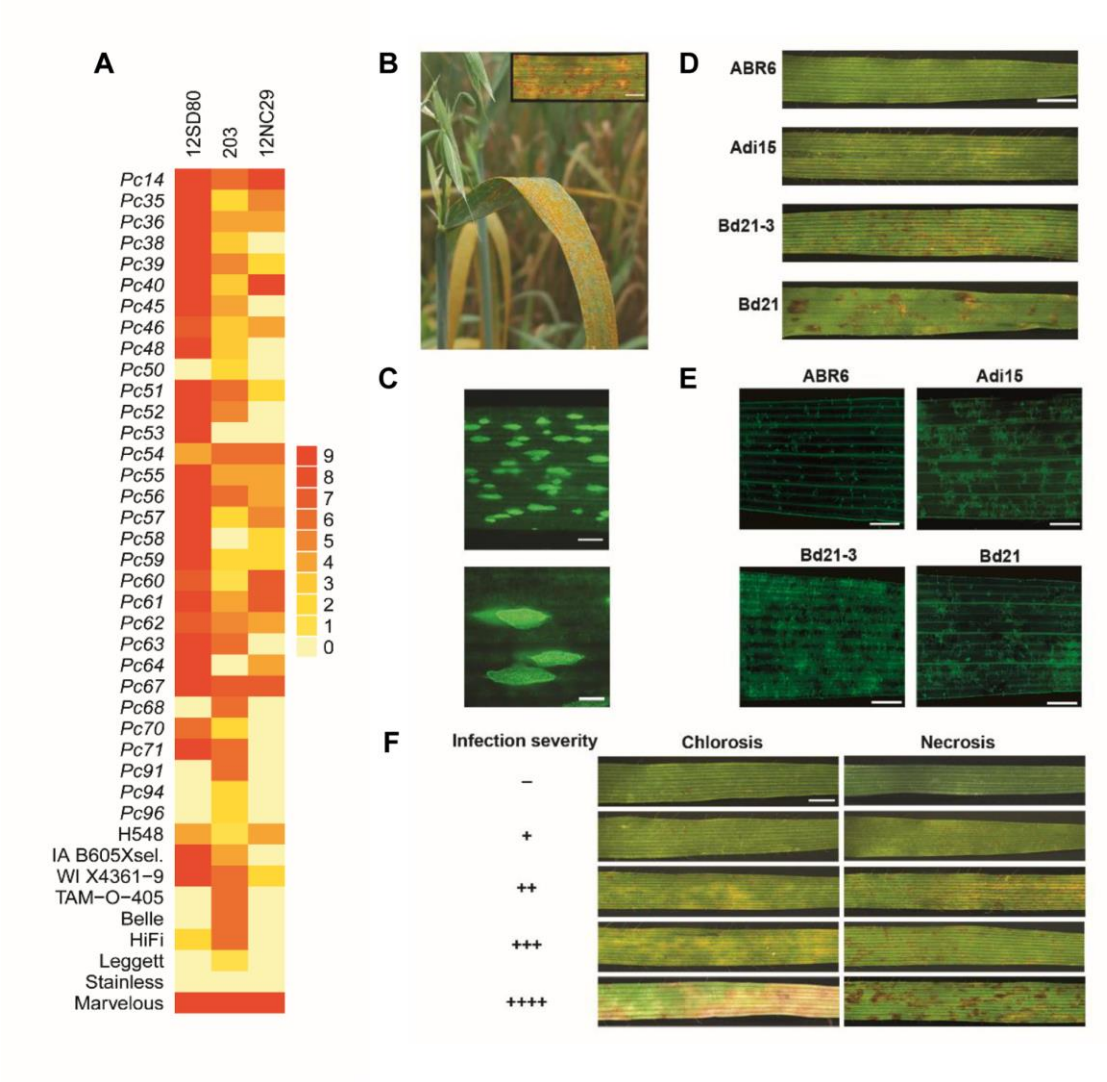

Fig. 1

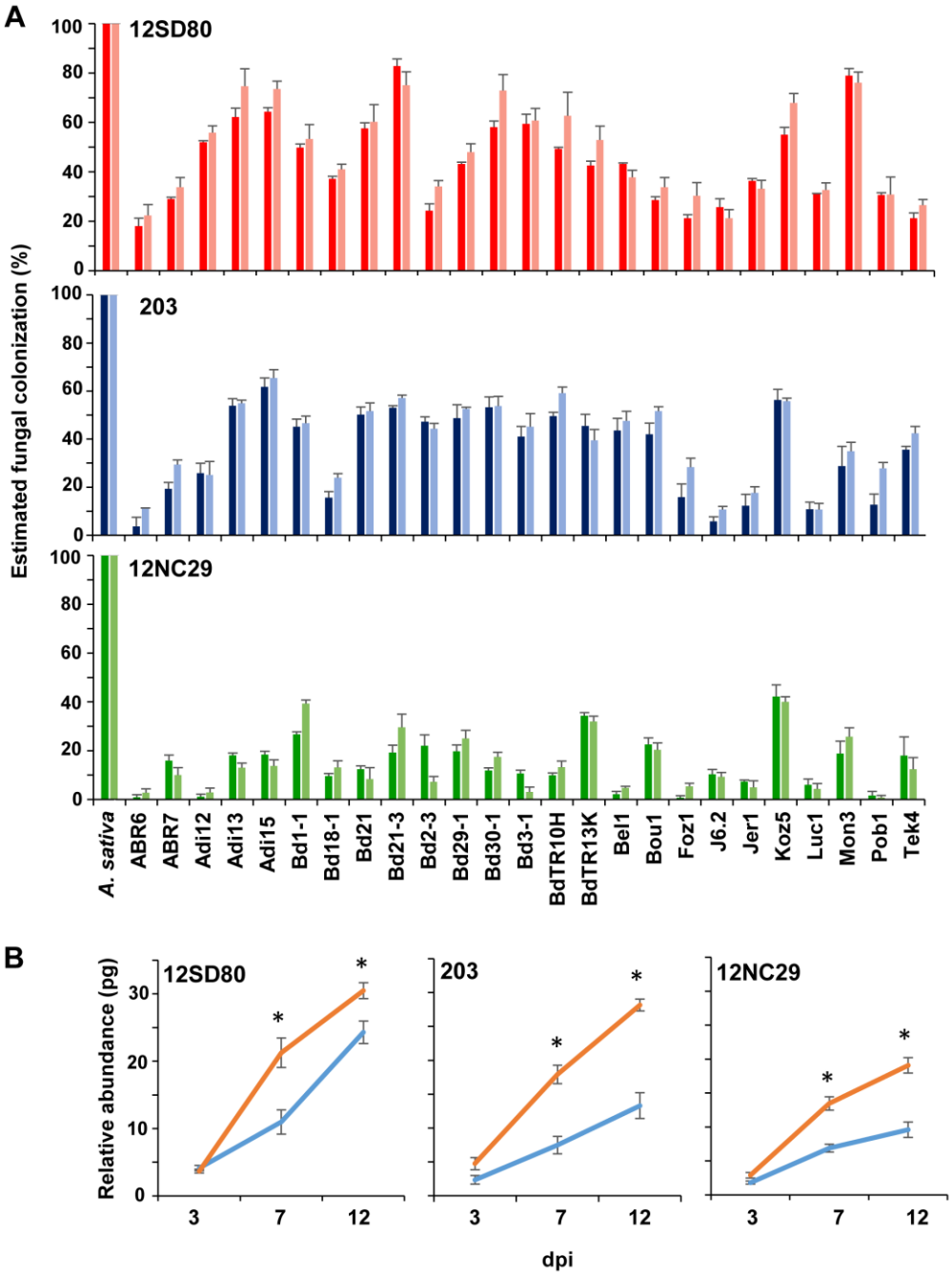

Fig. 2

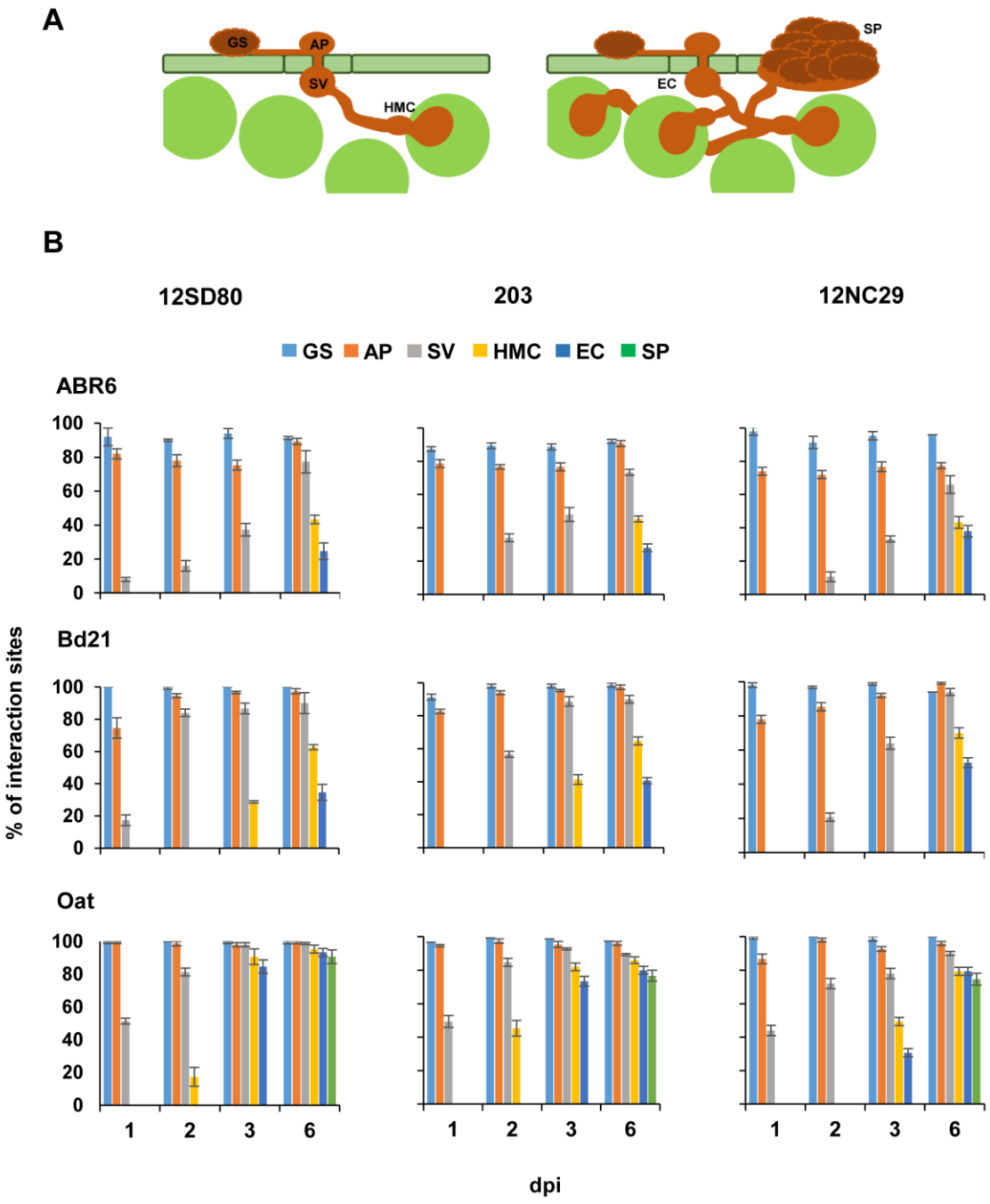

Fig. 3

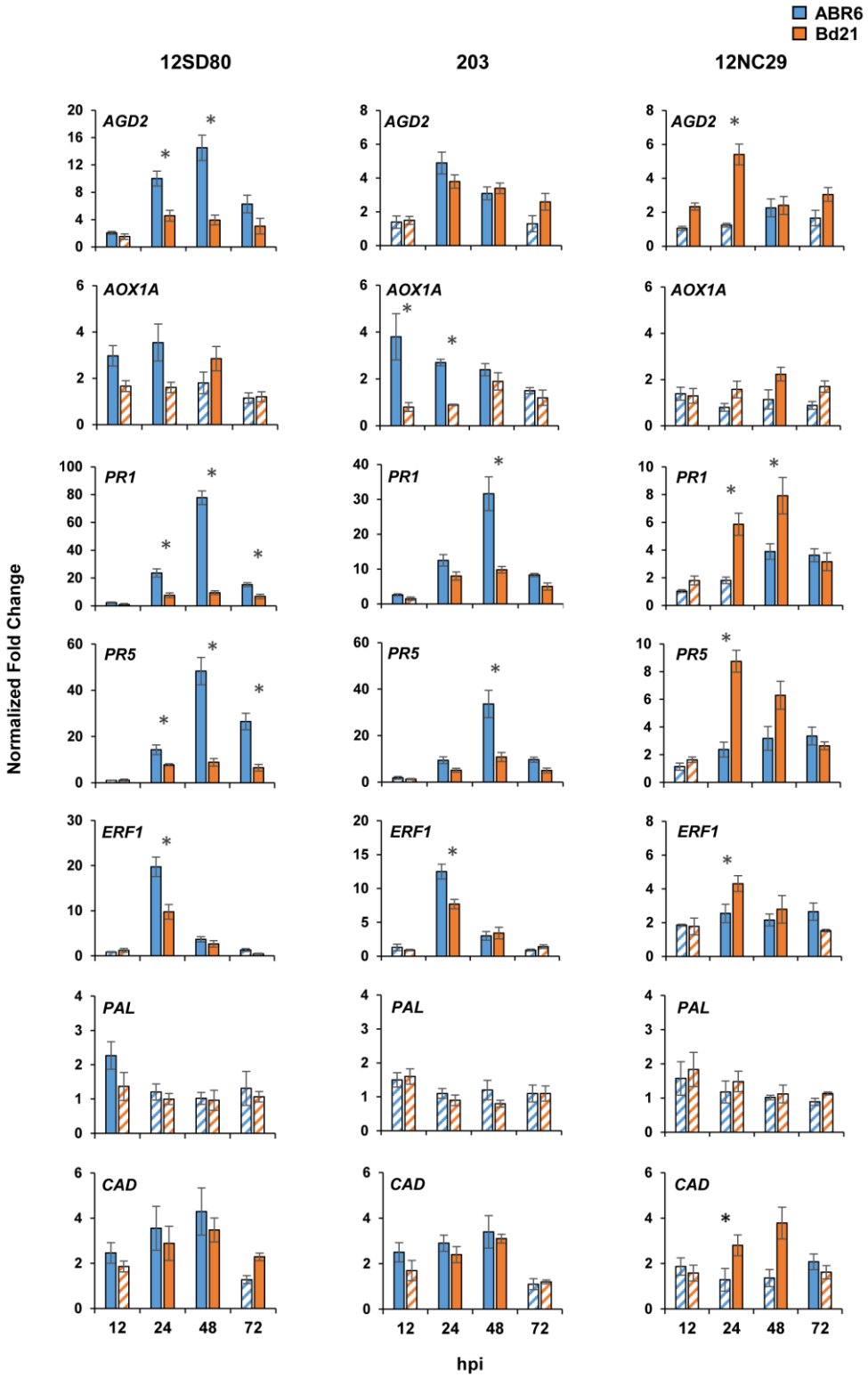

Fig. 4

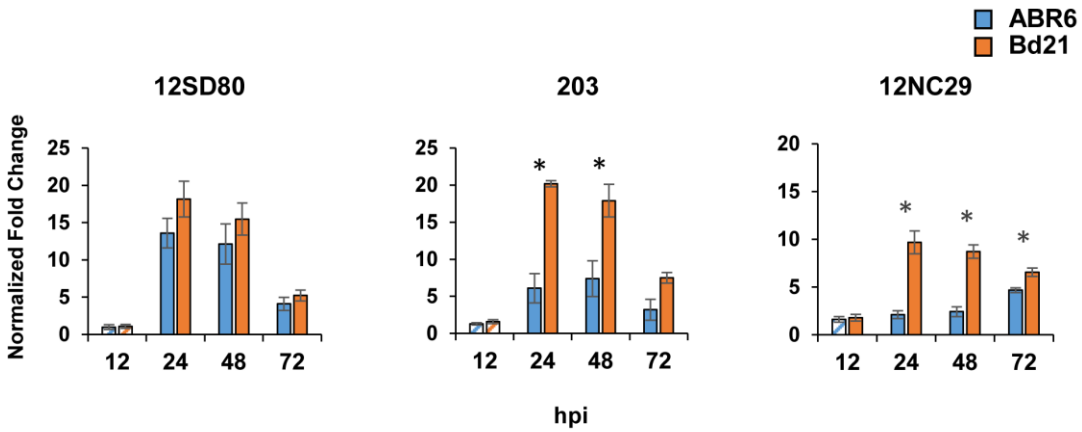

Fig. 5

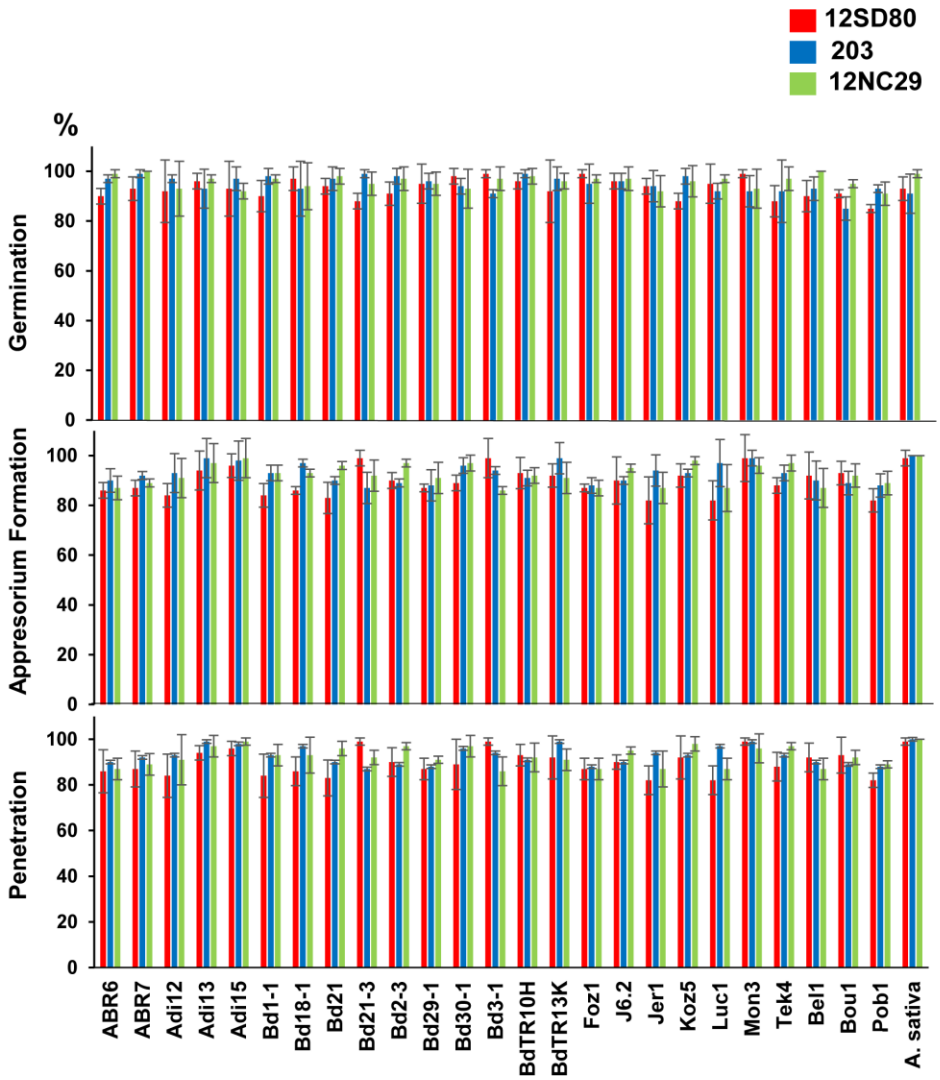

Supplementary Fig. 1

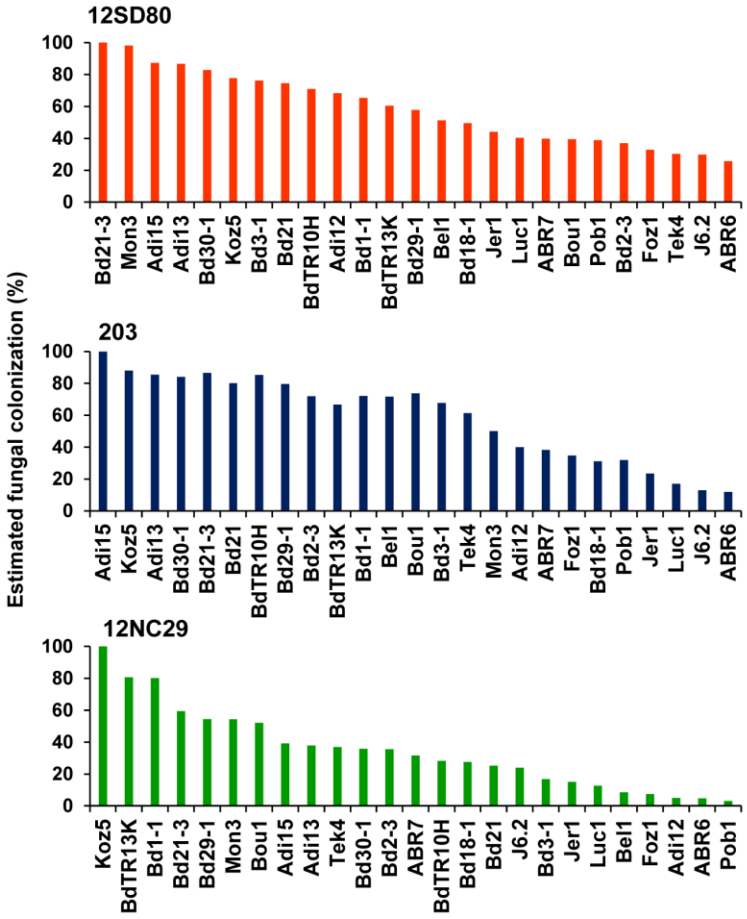

Supplementary Fig. 2

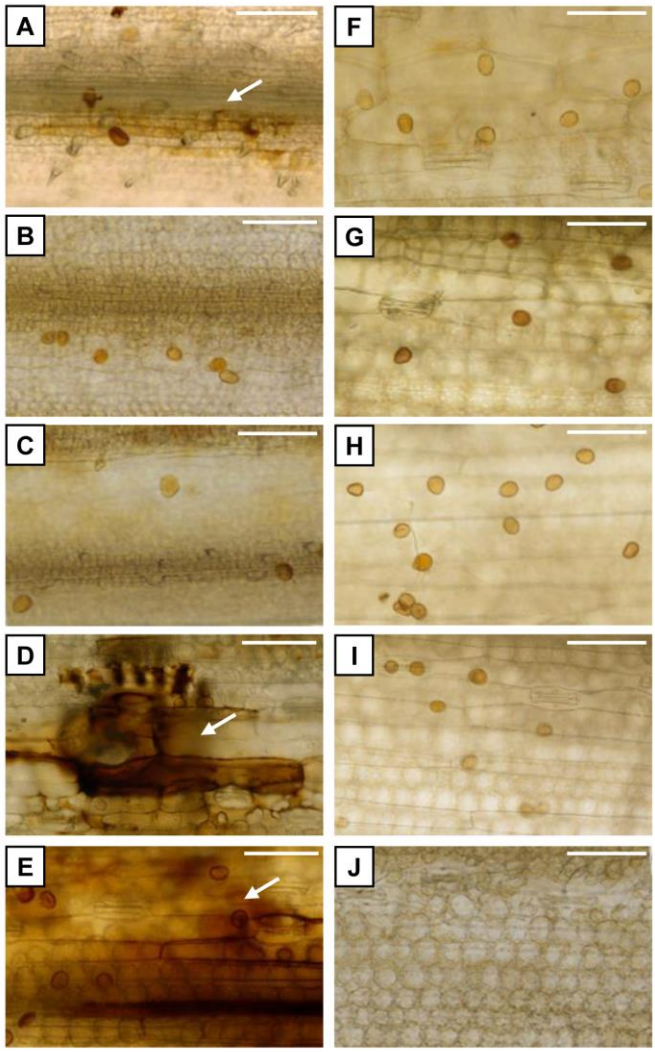

Supplementary Fig. 3

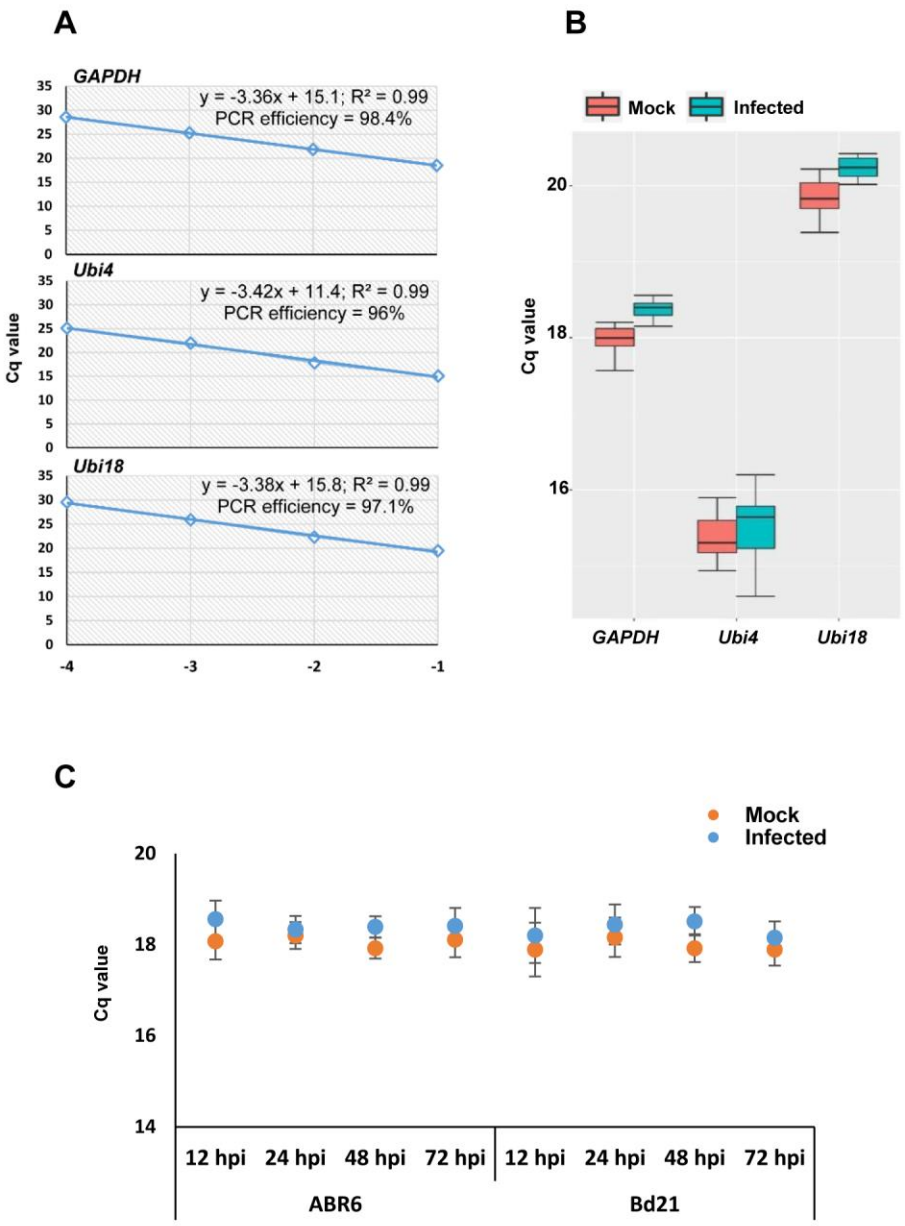

Supplementary Fig. 4

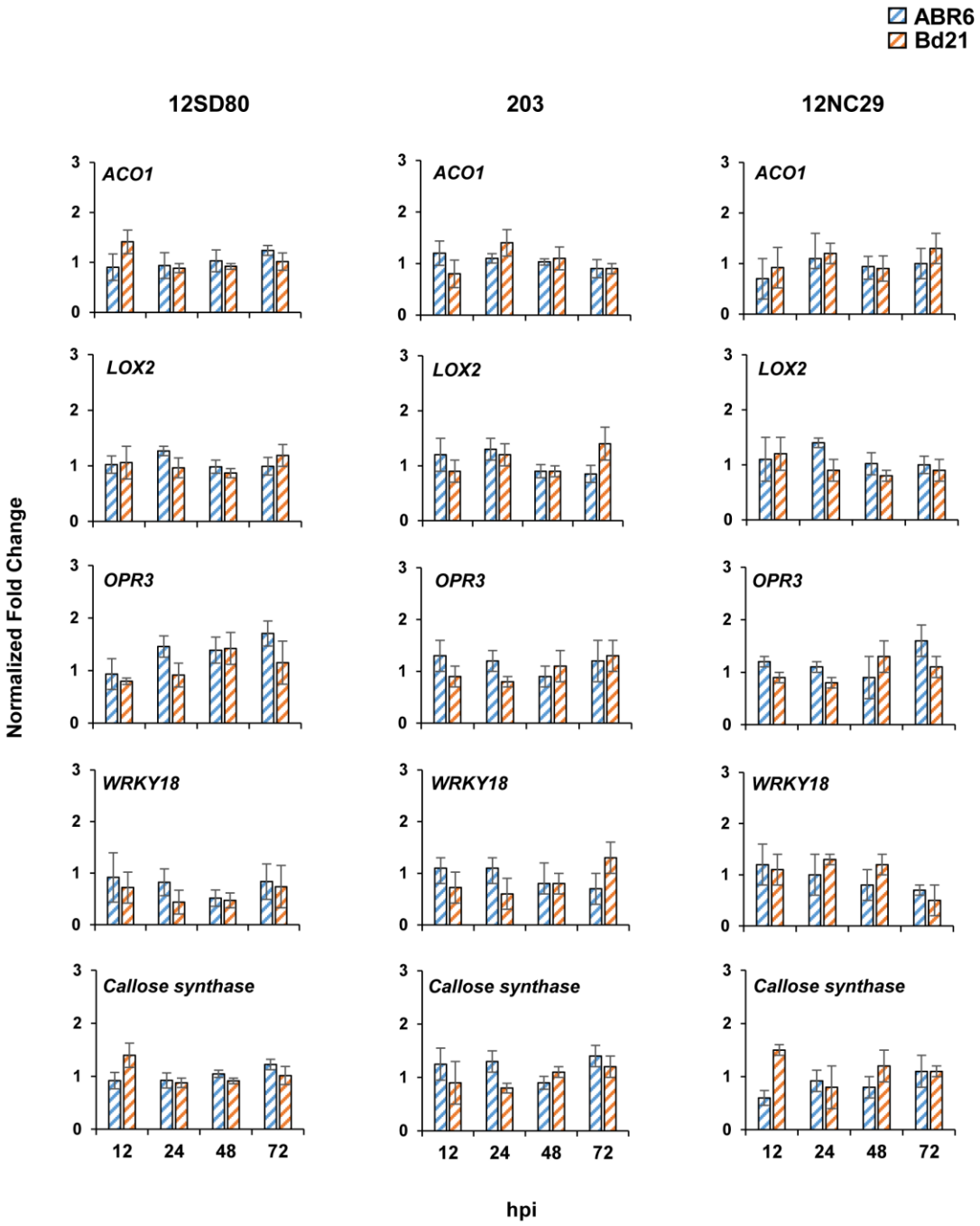

Supplementary Fig. 5